JGR Oceans

RESEARCH ARTICLE
10.1029/2022JC019592

Chimney-Like Intense Pelagic Upwelling in the Center of Basin-Scale Cyclonic Gyres in Large Lake Geneva

S. M. Hamze-Ziabari[1], U. Lemmin[1], M. Foroughan[1], R. S. Reiss[1], and D. A. Barry[1]

[1]Ecological Engineering Laboratory (ECOL), Institute of Environmental Engineering (IIE), Faculty of Architecture, Civil and Environmental Engineering (ENAC), Ecole Polytechnique Fédérale de Lausanne (EPFL), Lausanne, Switzerland

Key Points:

- Pelagic upwelling in the center of cyclonic gyres studied by 3D numerical modeling is confirmed by field measurements and remote sensing imagery
- Chimney-like pelagic upwelling that reached the surface was induced by cyclonic gyres in the surface mixed layer during summer and winter
- The 3D ageostrophic strain field caused by gyre distortion, not Ekman pumping, produced a dome-shaped thermocline and upwelling in the pelagic zone

Supporting Information:

Supporting Information may be found in the online version of this article.

Correspondence to:

S. M. Hamze-Ziabari,
mahmood.ziabari@epfl.ch

Citation:

Hamze-Ziabari, S. M., Lemmin, U., Foroughan, M., Reiss, R. S., & Barry, D. A. (2023). Chimney-like intense pelagic upwelling in the center of basin-scale cyclonic gyres in large Lake Geneva. *Journal of Geophysical Research: Oceans*, *128*, e2022JC019592. https://doi.org/10.1029/2022JC019592

Received 19 DEC 2022
Accepted 11 JUL 2023

Author Contributions:

Conceptualization: S. M. Hamze-Ziabari, U. Lemmin, D. A. Barry
Data curation: S. M. Hamze-Ziabari
Formal analysis: S. M. Hamze-Ziabari, U. Lemmin
Funding acquisition: D. A. Barry
Investigation: S. M. Hamze-Ziabari, M. Foroughan
Methodology: S. M. Hamze-Ziabari, U. Lemmin, M. Foroughan, R. S. Reiss
Project Administration: D. A. Barry

Abstract Basin-scale quasi-geostrophic gyres are common features of large lakes subject to Coriolis force. Cyclonic gyres are often characterized by dome-shaped thermoclines that form due to pelagic upwelling that takes place in their center. At present, the dynamics of pelagic upwelling within the surface mixed layer (SML) of large lakes are poorly documented. A unique combination of high-resolution 3D numerical modeling, satellite imagery and field observations allowed confirming, for the first time in a lake, the existence of intense pelagic upwelling in the center of cyclonic gyres under strong shallow (summer) and weak deep (winter) stratified conditions/thermocline. Field observations in Lake Geneva revealed that surprisingly intense upwelling from the thermocline to the SML and even to the lake surface occurred as chimney-like structures of cold water within the SML, as confirmed by Advanced Very High-Resolution Radiometer data. Results of a calibrated 3D numerical model suggest that the classical Ekman pumping mechanism cannot explain such pelagic upwelling. Analysis of the contribution of various terms in the vertically averaged momentum equation showed that the nonlinear (advective) term dominates, resulting in heterogeneous divergent flows within cyclonic gyres. The combination of nonlinear heterogeneous divergent flow and 3D ageostrophic strain caused by gyre distortion is responsible for the chimney-like upwelling in the SML. The potential impact of such pelagic upwelling on long-term observations at a measurement station in the center of Lake Geneva suggests that caution should be exercised when relying on limited (in space and/or time) profile measurements for monitoring and quantifying processes in large lakes.

Plain Language Summary Understanding the dynamics of Pelagic Upwelling (PU) is important because it can rapidly transport nutrients upwards from the thermocline into the phototrophic zone and thus can affect the biogeochemical balance of the lake. In large lakes subject to Coriolis force, pelagic upwelling in the center of cyclonic gyres has been observed. At present, little is known about PU within lakes because the processes associated with PU cannot be captured by the low-resolution numerical models typically used to investigate geostrophic processes, and high-resolution field observations are lacking. Here, high-resolution field measurements were combined with 3D numerical simulations and satellite imagery to investigate the PU structure in the center of a cyclonic gyre in Lake Geneva under different stratifications. Field observations documented, for the first time in a lake, details of the 3D velocity and temperature fields in cyclonic gyres. They showed that PU forms a chimney-like structure of cold water in the center of a cyclonic gyre. The chimney originates in the thermocline layer and can reach the lake surface, as confirmed by satellite images. As the thermocline descends during the cooling season, the chimney-like upwelling can attain a height of 80 m.

1. Introduction

In most thermally stratified large lakes subject to the Coriolis force, differential wind action across the surface causes basin-scale gyres to form (Akitomo et al., 2009; Beletsky et al., 1999; Csanady, 1973; Huttula & Sarvala, 2012; Lemmin & D'Adamo, 1996; Shimizu et al., 2007; Simons, 1980). Gyres are large-scale coherent circulations that play a critical role in the vertical and horizontal transport of nutrients, dissolved inorganic carbon, heat, sediment and algae in large lakes (Ishikawa et al., 2002; Ji & Jin, 2006). The interplay of vertical density stratification, Coriolis force, and irregularity in basin shape affects the formation of gyres (Mortimer, 2004; Valerio et al., 2017). Depending on the sign of the rotation, gyres can be characterized either by positive vorticity and a high-pressure core (cyclonic gyre) or negative vorticity and a low-pressure core (anticyclonic gyre). Basin-scale counterclockwise rotating (cyclonic) gyres are ubiquitous in most large Northern Hemisphere lakes (e.g., Beletsky & Schwab, 2008; Csanady, 1973; Laval et al., 2005); however, clockwise rotating (anticyclonic) gyres can also be formed due to Ekman pumping driven by anticyclonic vorticity in surface winds (e.g., Beletsky

Software: S. M. Hamze-Ziabari, R. S. Reiss
Supervision: U. Lemmin, D. A. Barry
Validation: S. M. Hamze-Ziabari
Visualization: S. M. Hamze-Ziabari, U. Lemmin
Writing – original draft: S. M. Hamze-Ziabari
Writing – review & editing: U. Lemmin, R. S. Reiss, D. A. Barry

et al., 2013). In the present study, we focus on cyclonic gyres, in particular on pelagic upwelling in their center, and investigate their dynamics during different seasons in Lake Geneva.

A basin-scale cyclonic circulation in most thermally stratified lakes is accompanied by a dome-shaped thermocline having a shallower depth in the center of the lake than at the nearshore (Csanady, 1968, 1977). Cold cores have been often observed/modeled in the center of these cyclonic circulations (e.g., Corman et al., 2010; McKinney et al., 2012; Ralph, 2002; Romanovsky & Shabunin, 2002; Troitskaya et al., 2015). On the other hand, a bowl-shaped thermocline (i.e., deeper in the center of the lake and shallower in the nearshore) can be formed within an anticyclonic gyre (Beletsky et al., 2012). Resulting physical processes such as upwelling and downwelling in the coastal and pelagic areas of lakes can significantly affect the functioning of the lake ecosystem (Corman et al., 2010; Ostrovsky & Sukenik, 2008) by changing the physical (e.g., temperature, currents) and chemical (e.g., pollution, salinity) conditions of the water column and, consequently, biological processes such as phytoplankton growth and bacterial life cycles (Lovecchio et al., 2022; Troitskaya et al., 2015). The vertical motions associated with gyre dynamics can locally transport nutrients from the metalimnion and hypolimnion into the epilimnion layer, potentially creating hot spots of biological activity (Corman et al., 2010; Romanovsky & Shabunin, 2002; Troitskaya et al., 2015).

Previous studies suggested two physical mechanisms to explain the formation of pelagic upwelling at the center of a cyclonic circulation during summertime: (a) differential heating (baroclinic effect) and (b) Ekman transport caused by cyclonic surface winds. Using a conceptual model, Csanady (1977) analyzed the combined effect of wind stress drift and differential heating in nearshore-offshore regions, where shallow nearshore regions warm faster than deeper mid-lake regions. For Lake Ontario, this combination produced a dome-shaped thermocline during summer. Baroclinic effects due to a dome-shaped thermocline can generate a pressure gradient between the mid-lake and nearshore regions, which can lead to/contribute to the formation of cyclonic circulations (Beletsky et al., 2013). However, a numerical study by Schwab et al. (1995) showed that imposing a zero-heat flux condition at a sloping lake boundary can also form a dome-shaped thermocline.

Dome-shaped thermoclines can also be generated by the divergence of Ekman transport, that is, Ekman pumping, caused by cyclonic wind stress curl (Gill, 1982). Although observational evidence for Ekman pumping is rare in physical limnology, wind stress curl has been reported over many large lakes (e.g., Lake Superior (Bennington et al., 2010); Lake Michigan (Schwab & Beletsky, 2003); Lake Biwa (Japan; Endoh et al., 1995); Lake Tahoe (USA; Strub & Powell, 1986); Lake Geneva (Lemmin & D'Adamo, 1996), suggesting that such a mechanism may contribute to the formation of dome- or bowl-shaped thermoclines. In the pelagic region, cyclonic/anticyclonic wind fields cause near-surface divergence/convergence and surface-level depression/elevation, which in turn creates a dome-shaped/bowl-shaped thermocline induced by upwelling/downwelling in the mid-lake region. The "deformed" thermocline and the water surface level change produced by such a process can result in horizontal pressure gradients, which can contribute to the formation of pelagic cyclonic or anticyclonic circulations.

Nearshore upwelling has been investigated in various lakes (e.g., Corman et al., 2010; Flood et al., 2020; Plattner et al., 2006; Pöschke et al., 2015; Reiss et al., 2020; Rowe et al., 2019; Valbuena et al., 2022). However, few studies have reported on dome- or bowl-shaped thermoclines in lakes and pelagic upwelling/downwelling during summer (e.g., Beletsky et al., 2012). Field observations conducted in Lake Issyk-Kul (Kirgistan) showed that an increase of dissolved oxygen in the surface layer occurs in the pelagic upwelling zone (Romanovsky & Shabunin, 2002). In Lake Tanganyika (Africa), Corman et al. (2010) found that pelagic upwelling can strongly affect the temporal pattern of temperature, nutrients, and phytoplankton chlorophyll. More recently, Troitskaya et al. (2015) used in situ and remote sensing data to identify pelagic upwelling in Lake Baikal (Russia) during summer.

Sparse, previous pelagic upwelling field observations in lakes were typically limited to at most a few moorings. Thus, they cannot provide a direct, detailed description of large-scale gyre patterns and the associated pelagic upwelling (Beletsky et al., 2013; Hui et al., 2021). Although upwelling and downwelling in the center of basin-scale gyres are well known from theory, there are no reports of the transport of thermocline water to the epilimnion or even to the lake surface caused by pelagic upwelling. This is likely due to: (a) the difficulty of taking detailed, high-resolution field observations of temperature profiles and velocity fields that can confirm the existence of such patterns, and (b) the fact that pelagic upwelling cannot be captured by the low-resolution numerical models often used to investigate geostrophic processes in large lakes (Brannigan, 2016). Lu et al. (2020) demonstrated in theory that in the ocean, a Tropical Cyclone (TC) can cause vertical perturbations in the surface mixed layer (SML) of cyclonic and anticyclonic eddies, and a

chimney-like upwelling, that is, a cylinder of well-mixed cold water, can appear in the Ekman layer. However, a cyclonic wind stress of TC intensity is rare over most lakes. Unlike convective chimneys reported in the literature where strong heat fluxes from the sea surface combined with cyclonic circulation cause downward transport (Kovalevsky et al., 2020), chimney-like pelagic upwelling, the subject of this study, produces upward transport.

Using only surface data, previous studies have shown that pelagic upwelling in gyres and eddies exists in lakes. Infrared and optical sensors such as the Advanced Very High-Resolution Radiometer (AVHRR) are often applied to distinguish the signatures of coastal and pelagic upwelling in lakes and oceans (Gutiérrez et al., 2011; Pisoni et al., 2014). McKinney et al. (2012), using AVHRR and synthetic aperture radar data, reported cold cores in cyclonic eddies (diameter ∼17 km) in the nearshore zone of Lake Superior, suggesting pelagic upwelling. However, detailed field measurements are lacking. In particular, vertical dynamics associated with cyclonic gyres in the absence of cyclonic wind stress have not been studied in lakes. Therefore, in order to help fill this knowledge gap, we investigate here the formation of a chimney-like pelagic upwelling in the SML of Lake Geneva in the absence of wind during the development and propagation of gyres. Lake Geneva exhibits frequent and predictable cyclonic and anticyclonic gyres after strong wind events (Hamze-Ziabari, Lemmin, et al., 2022), thus making it an ideal site to investigate vertical transport associated with gyres. For this, spatially detailed in situ measurements of temperature and velocity profiles accompanied by high-resolution three-dimensional (3D) numerical modeling and remote sensing (AVHRR) imagery were employed to capture the cyclonic circulation and associated intense upwelling during both the strongly and weakly stratified seasons. The following questions are addressed.

- Can field measurements confirm the detailed temperature and current structure of a cyclonic gyre in the center of the lake that was predicted by high-resolution 3D modeling?
- How stable are the gyre and the pelagic upwelling in time and space?
- What effect does the seasonal change in stratification have on the development of the gyre and the pelagic upwelling?
- Is the dome-shaped thermocline and pelagic upwelling caused by Ekman pumping? If not, what alternative processes can explain them?
- What is the potential impact of such upwelling on vertical profile data collected at a long-term monitoring station located in the area where the strongest pelagic upwelling is detected?

The Supplementary Information (SI) section provides complementary texts and figures identified with prefix S.

2. Materials and Methods

2.1. Field Site

Lake Geneva (local name: *Lac Léman*), the largest lake in Western Europe, is located between Switzerland and France (Figure 1a). It is composed of two basins: the large *Grand Lac* in the east (maximum depth 309 m), and the small, narrow *Petit Lac* in the west (maximum depth ∼70 m). The lake has a surface area of 580 km^2, a volume of 89 km^3, and a length of ∼70 km along its main arc. Its maximum width is 14 km. The lake is surrounded by the Alps to the south and east, and the Jura mountains to the northwest. Due to the mountainous topography of the surrounding area, there are two strong dominant wind fields, the *Bise* coming from the northeast and the *Vent*, from the southwest. The central and western parts of the lake are frequently subject to strong winds, which can last several hours to several days. However, the eastern part of the lake is sheltered from strong winds by high mountains (Lemmin & D'Adamo, 1996; Lemmin, 2020; Rahaghi et al., 2019). The Rossby radius of deformation for stratified Lake Geneva has been estimated to be 5 ± 0.5 km (Bauer et al., 1981; Cimatoribus et al., 2018; Hamze-Ziabari, Razmi, et al., 2022; Lemmin et al., 2005) indicating that the Coriolis force is important in the force balance.

The spatial pattern of the averaged *Bise* and *Vent* wind fields is shown in Figures 1b and 1d. These strong uniform wind events can generate complex gyral flow pattern systems (Figures 1c and 1e). The surface currents in the lake's center are either cyclonic (counterclockwise rotating) after a *Bise* wind or anticyclonic (clockwise rotating) after a *Vent* event (Hamze-Ziabari, Lemmin, et al., 2022; Lemmin, 2016). In order to monitor the long-term water quality development of the lake, the Commission Internationale pour la Protection des Eaux du Léman (CIPEL) has measured physical and biological parameters regularly since 1967 at station SHL2 (Figure 1a).

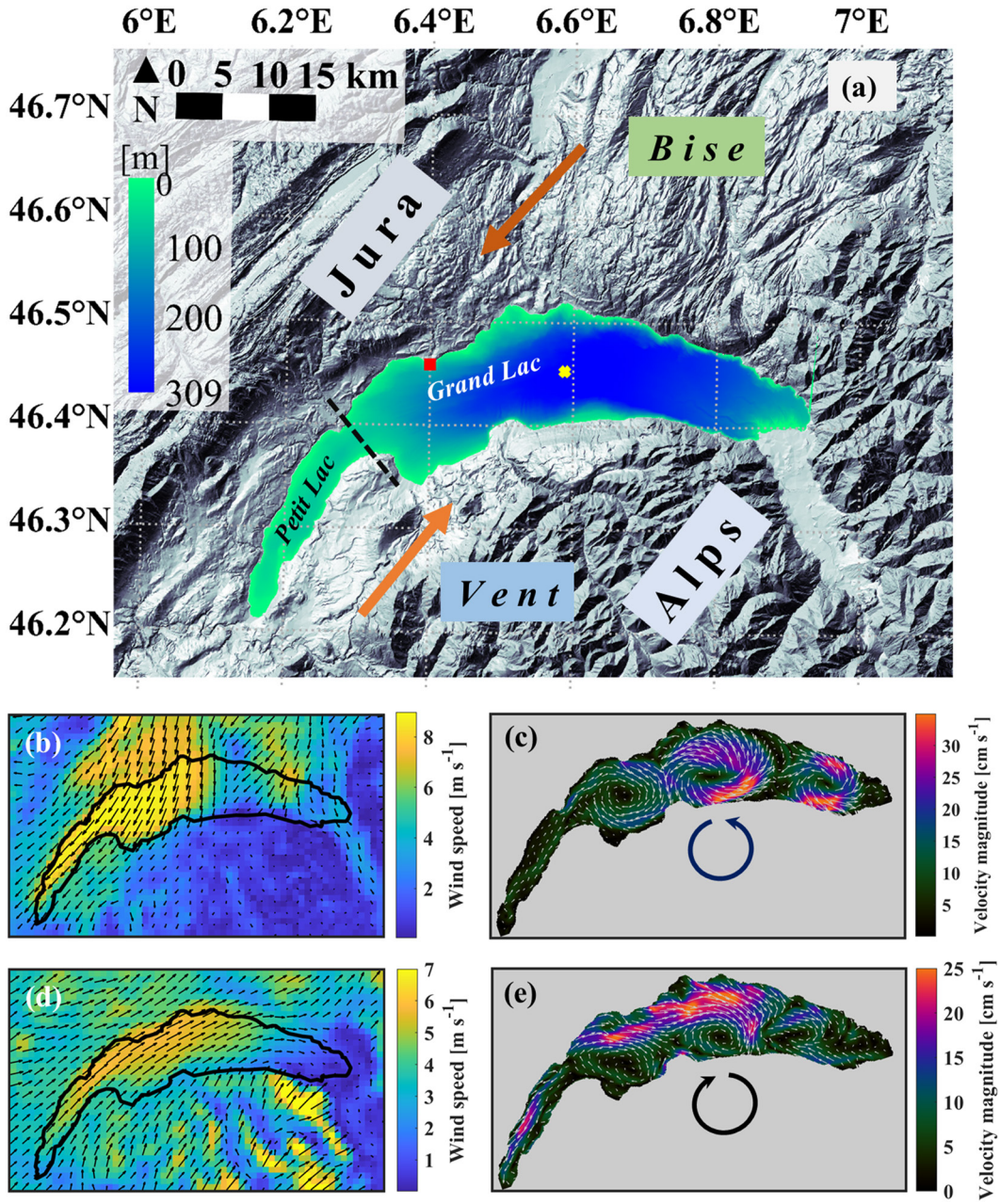

Figure 1. (a) Lake Geneva and surrounding topography, adapted from a public domain satellite image (NASA World Wind, last accessed 13 December 2022) and bathymetry data from SwissTopo (last accessed 13 December 2022). The colorbar indicates the water depth. SHL2 (yellow cross) is a long-term CIPEL monitoring station where physical and biological parameters are measured; red square: location of the EPFL Buchillon meteorological station (100-m offshore). The thick brown arrows indicate the direction of the two strong dominant winds, called *Bise*, coming from the northeast and *Vent*, from the southwest. (b) Average wind speed and direction during the *Bise* event that lasted from 18–20 September 2019. (c) Magnitude of simulated near-surface current velocity patterns 1 day after the *Bise* ceased. A cyclonic gyre formed in the center (widest part) of the *Grand Lac* basin of the lake (black circular arrow) and is part of the three-gyre pattern. (d) Average wind speed and direction during the *Vent* event that lasted from 24–30 September 2019. (e) Near-surface (simulated) flow patterns 1 day after the *Vent* ceased. An anticyclonic gyre formed in the center (widest part) of the *Grand Lac* basin (black circular arrow). Colorbars indicate the range of the parameters.

2.2. Numerical Simulations

We investigated the 3D processes involved in pelagic upwelling using the Massachusetts Institute of Technology general circulation model (MITgcm). This code solves the 3D Boussinesq, hydrostatic Navier-Stokes equations,

including the Coriolis force (Marshall et al., 1997). Given the minor role of salinity in the determination of density in Lake Geneva, it is fixed at 0.05 psu. Density changes are then due to temperature variations, which are accounted for in the model (Cimatoribus et al., 2018). In addition, the model considers the effects of free-surface elevation, which significantly influence the hydrodynamic behavior of the lake. We applied the model setup of Cimatoribus et al. (2018, 2019) who calibrated the model for Lake Geneva and demonstrated that stratification, mean flow and internal seiche variability can be realistically simulated. In addition, Foroughan et al. (2022), Hamze-Ziabri, Fouroughan, et al., 2022), Hamze-Ziabari, Lemmin, et al. (2022), Hamze-Ziabri, Razmi, et al. (2022), and Reiss et al. (2020, 2022, 2023) showed that the model can accurately capture both submesoscale and basin/mesoscale processes in Lake Geneva. Realistic atmospheric fields (including wind, temperature, humidity, solar radiation), extracted from the COnsortium for Small-scale MOdeling (COSMO) atmospheric model provided by MeteoSwiss with a resolution of 1 km (Voudouri et al., 2017), were used to force the lake surface. The K-Profile Parameterization scheme, a widely used non-local vertical-mixing parameterization, was employed to simulate turbulent processes in the lake.

Two Cartesian grids, a Low Resolution (LR) grid (horizontal resolution 173–260 m, 35 depth layers) and a High Resolution (HR) grid (horizontal resolution 113 m, 50 depth layers), were applied. The LR model was initialized from rest using the temperature profile from CIPEL station SHL2 (CIPEL, 2018) measured on 19 December 2018 (calm weather conditions prevailed on this date). The LR model spin-up was ∼180 days. Note that the LR results were only used to initialize the HR model. The layer thicknesses in the HR model ranged from 0.30 m at the surface to approximately 12 m for the deepest layer and the integration time was 6 s.

2.3. Remote Sensing

The signatures of coastal and pelagic upwelling in lakes and oceans are usually detected using infrared and optical sensors. Advanced Very High-Resolution Radiometer data from the National Oceanic and Atmospheric Administration and the European Meteorological Operational (MetOp) polar-orbiting satellites, which are routinely collected by the Remote Sensing Research Group at the University of Bern (Riffler et al., 2015), were used to study the spatial variability of pelagic upwelling events in Lake Geneva. Advanced Very High-Resolution Radiometer data have a spatial resolution of 1.1 km at nadir and a temporal resolution of one to 10 images per day (Bouffard et al., 2018; Rahaghi et al., 2018). Detailed information is provided by Hüsler et al. (2011) and Riffler et al. (2015).

2.4. In Situ Data

It was previously shown that gyre patterns in Lake Geneva can be reliably predicted by numerical modeling based on forecasted COSMO meteorological data (Hamze-Ziabari, Lemmin, et al., 2022). Guided by these numerical model forecasts, one or more transects for field measurements were selected within the main cyclonic gyre in the central part of the *Grand Lac* basin. Ten 1 km-spaced profiles were measured along the transect. An ADCP (Acoustic Doppler Current Profiler, Teledyne Marine Workhorse Sentinel) equipped with a bottom-tracking module was used to measure the vertical profiles of current velocity at each point for at least 10 min. The ADCP was set up for 100 1-m bins (blanking distance of 2 m). The transducer was located at 0.5 m depth, and the high-resolution processing mode was chosen. Tilt and heading angles were derived from an in-built sensor.

Vertical profiles of water temperature were measured with a multiparameter probe Sea and Sun Marine Tech CTD75M and CTD90M at predefined points during the field campaigns. The conductivity temperature depth instrument was lowered at ∼10 cm s^{-1} and recorded at 7 Hz, resulting in a sampling resolution of ∼1.5 cm.

2.5. Empirical Orthogonal Functions

Empirical Orthogonal Function (EOF) analysis is widely used to identify latent spatial patterns in a data set and how they change over time (Wang & An, 2005). In an EOF analysis, similar to Fourier or wavelet analysis, the original data set is projected onto an orthogonal basis. This orthogonal basis is computed based on the eigenvectors of a spatially weighted anomaly covariance matrix. The associated eigenvalues are a measure of the variance captured by each pattern. Let $X = \{x(t_1), x(t_1),\ldots, x(t_N)\}$ be an $(n \times m)$ matrix of numerical results, where m is the number of grid points in each spatial output (x) and N is the number of time snapshots. The covariance matrix of X is given by:

$$C = \frac{1}{m-1}(X - \langle X\rangle)(X - \langle X\rangle)^T \quad (1)$$

where $\langle X \rangle$ is the space-dependent temporal mean of X. The eigenvalue problem is:

$$CV = V\lambda \tag{2}$$

where V is an eigenvector of C and λ is its corresponding eigenvalue. The eigenvectors of C, represented by the columns of V, are called empirical orthogonal functions (EOFs). The eigenvalues (PCs) of C, represented by the diagonal entries of λ, are proportional to the variance quantified by each EOF.

A thermocline with a dome- or bowl-shaped structure associated with pelagic upwelling and downwelling, respectively, produces a coherent structure in the temperature field. The thermocline layer is primarily affected by pelagic and coastal upwelling, which can result in significant spatial variability of temperature. In contrast, atmospheric forcing has a lesser impact on this layer. The pelagic upwelling/downwelling events can persist from days to weeks, depending on the strength and persistence of wind events (Hamze-Ziabari, Lemmin, et al., 2022). By analyzing the EOFs of the temperature in the thermocline layer, it is therefore possible to determine the spatial variability of temperature induced by such processes.

2.6. Ekman Pumping Velocity

Wind-driven upwelling can occur in both coastal and offshore areas of lakes and oceans. In coastal upwelling, surface waters are transported away from the alongshore direction due to Ekman transport. This generates near-shore divergence in the surface layers, which is balanced by the upwelling of colder waters from below (Reiss et al., 2020). Upwelling in offshore areas can be caused by the divergence of Ekman mass transport, which results from the curl of the wind stress. The Ekman pumping velocity induced by wind stress is given by (Bravo et al., 2016; Pickett & Paduan, 2003):

$$W_{\text{Ekman pumping}} = \frac{\nabla \times \tau}{\rho f} \tag{3}$$

where $W_{\text{Ekman pumping}}$ is the Ekman pumping velocity, τ is the wind stress, ρ is the water density and f is the Coriolis frequency. The wind stress at the air-water interface was calculated from hourly COSMO data as:

$$\tau = (\tau_x, \tau_y) = \rho_a C_D \Delta\vec{U} |\Delta\vec{U}| \tag{4}$$

where τ_x is the zonal and τ_y is the meridional wind stress, $\Delta\vec{U} = \vec{U}(z_u) - \vec{U}_0$ is the difference between wind velocity vector at height z_u (typically 10 m) and the surface current. The drag coefficient at the air-water interface (C_D) was estimated as (Large & Yeager, 2004):

$$C_D\left(\times 10^3\right) = \frac{2.7}{U_{10N}} + 0.142 + 0.076 U_{10N} \tag{5}$$

where U_{10N} is the 10-m neutral-stability wind speed.

3. Results

3.1. Field Observations

This study focuses on *Bise* wind events that caused the formation of a cyclonic gyre and pelagic upwelling in the central region of the *Grand Lac* basin of Lake Geneva. This gyre is part of a three-gyre pattern that was previously identified as the typical response to strong *Bise* winds blowing over lake (Hamze-Ziabari, Lemmin, et al., 2022; Figure 1c). Pelagic upwelling is important for the ecological development of the lake, since it transports nutrients from the deeper layers into the phototrophic zone. For the field campaigns, emphasis was put on cases where modeling suggested that thermocline waters reach the surface. On 21 September 2019, a field measurement campaign was carried out whose primary objective was to capture the dynamics of the largest and most energetic basin-scale gyre in the center of the *Grand Lac*. A strong *Bise* event started at 20:00 (CET) on 17 September 2019 and ended at 13:00 on 20 September 2019. The mean wind speed was 3.65 ± 0.86 m s^{-1} (mean wind gust of 7.69 ± 1.78 m s^{-1}). Details of the wind field are given in Figure 1b and Figure S1 in Supporting Information S1. As shown in Figure 2a, this wind event produced three basin-scale gyres. Three transects in the central gyre, T1, T2 and T3, spaced at ~1.8–2 km distance (east to west), were pre-selected. Each transect consisted of

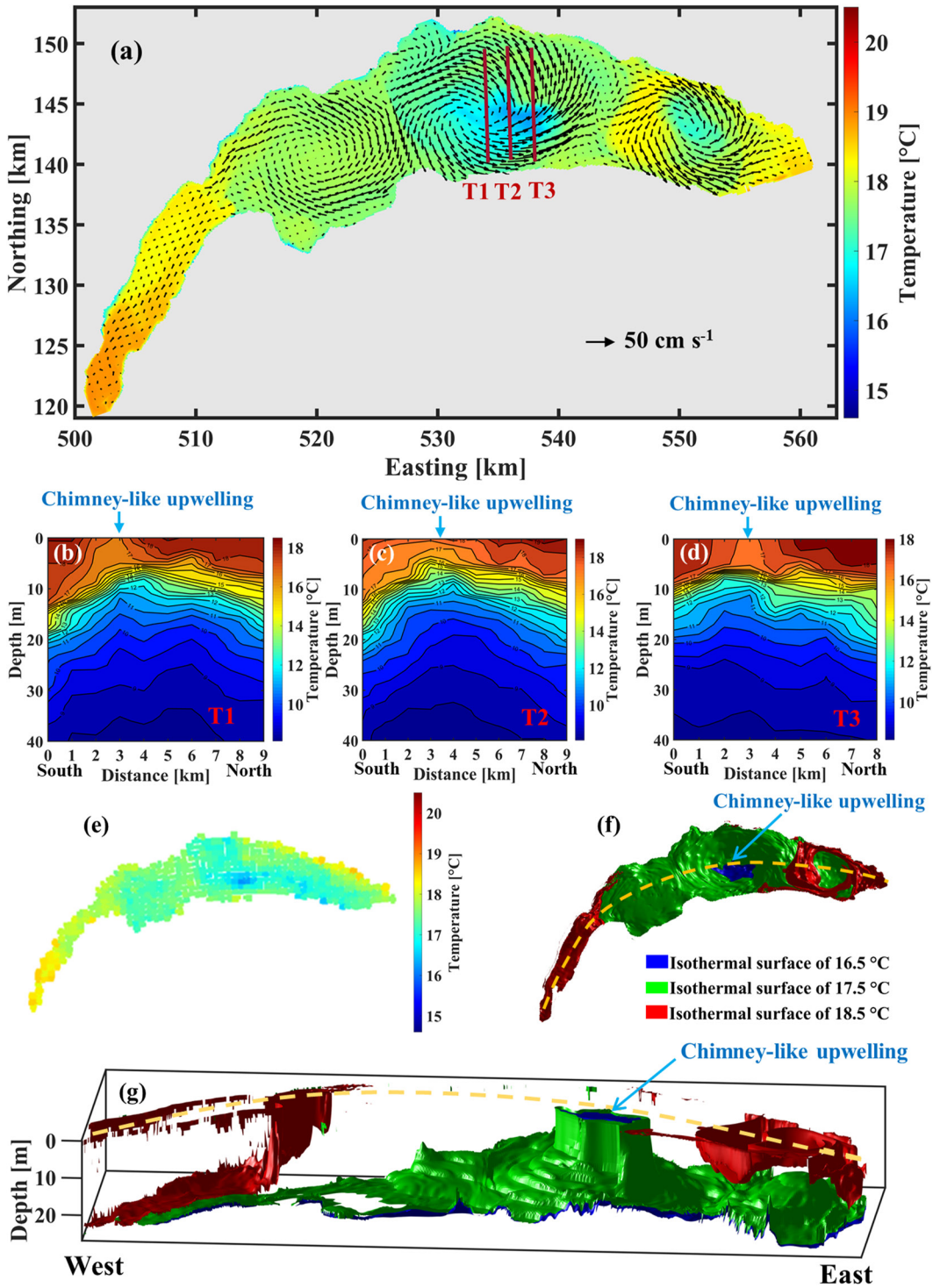

Figure 2. (a) Numerical results of the temperature (colorbar) and velocity (arrows) fields (0.3-m depth) for 21 September 2019 after the strong *Bise* wind event, showing two cyclonic gyres, in the center and to the east, and one anticyclonic gyre in the western part of the *Grand Lac*. The red parallel lines in the central cyclonic gyre mark the predefined field measurement transects (T1, T2, T3). (b–d) Contour plots based on the measured temperature profiles at T1, T2 and T3, respectively (colorbar gives the temperature range). (e) Advanced Very High-Resolution Radiometer image taken on 21 September 2019 at 8:21 with the same temperature range as in panel (a). The location of the cold temperature ellipse in the center (blue) coincides well with the one predicted by the numerical modeling (panel a). (f and g) 3D structure of three isothermal s,urfaces related to the upwelling zones in the numerical results. Isothermal surfaces of thermocline water that have depths of 10, 15, and 20 m in the nearshore areas are considered (compare with panels b–d): (f) plan view; (g) side view. Yellow dashed line in (f) indicates the central plane orientation in (g). Blue arrows in (f) and (g) mark the location of the pelagic upwelling in the center of the cyclonic gyre in the *Grand Lac* basin.

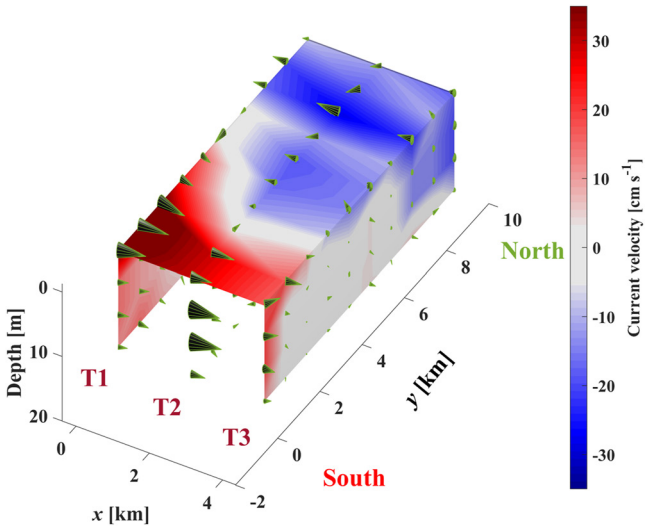

Figure 3. 3D structure of the cyclonic gyre velocity field based on the ADCP profiles taken during the field campaign of 21 September 2019 in Lake Geneva along transects T1, T2, and T3 shown in Figure 2a. The size of the arrows is scaled with the current velocity. Contours show the current velocities near the surface and on the sides of the investigated volume. Colorbar gives the range.

10 profiles with 1-km spacing (Figure 2a). Temperature profiles at each point were measured down to 40 m depth, that is, the base of the thermocline.

The velocity field shows a cyclonic gyre (Figure 3). The maximum horizontal water velocity reached ~35 cm s^{-1} in the near-surface layer. The upwelling in the center of the gyre was accompanied by a strong reduction of the horizontal velocity, which can be clearly observed in all transects. The gyre velocity field depth was slightly less than 15 m due to strong thermal stratification (Figures 2b–2d). However, the gyre affected the temperature profiles down to a depth of ~40 m. At depths below 10 m, the expected dome-shaped thermocline is evident in the temperature profiles (Figure 2b). It was observed that the cyclonic gyre circulation pushes the water from a depth of 10 m to the surface. As a result, the surface water temperature in the center of the gyre is 1–1.5ºC colder than the surrounding surface water, as seen in the T1 and T2 transects. Below, we refer to these vertical cold-water columns (e.g., between distances 2–3 km in Figure 2b) as chimney-like pelagic upwelling. These gyre features were not documented previously within lakes in such detail.

The lake surface water temperature field retrieved from AVHRR data with a spatial resolution of 1.1 km taken at 9:00 on 21 September 2019 (Figure 2e) shows an irregular ellipse-like cold area that is 1°C colder than the surrounding surface waters. The width of the ellipse is ~3 km and its length is ~5 km. A similar cold-water pattern at the same location with the same surface area is evident in the numerical results (Figure 2a), indicating that the model well predicts the observations. The 3D structure of the pelagic upwelling in the SML is illustrated by three isothermal surfaces of thermocline water at depths 10, 15 and 20 m in the nearshore areas (Figures 2f and 2g). In the center of the observed cyclonic gyre, the water from the thermocline reaches the surface and forms a chimney-like structure in the SML (Figure 2g). The 3D structure of isothermal surfaces related to these upwelling zones is consistent with the field measurements (Figures 2b–2d), thus confirming the existence of a cold chimney-like structure in the epilimnion layer, in which cooler water originating from the thermocline is transported upwards into the surface layer.

3.2. Evolution of Spatial Variability of Pelagic Upwelling During Strong Stratification

AVHRR data and numerical results are used to show the spatial variability of pelagic upwelling over the lifetime of the gyre observed in September 2019 (Figure 4). In the AVHRR images taken from 19–21 September 2019, it is evident that the location of pelagic cold areas and their geometric shape are quite variable in time. The same spatial variability of the pelagic upwelling can be seen in the corresponding numerical results, indicating reasonable agreement with AVHRR data. On 19 and 20 September, the velocity fields in the numerical modeling present a gyre-like pattern located in the south (Figures 4b and 4d). On 21 September, the modeled gyre velocity field was fully developed and nearly symmetrical with respect to the center of the lake with the cold upwelling zone also shifting toward the lake center. The AVHRR and numerical results indicate that the cold surface areas correspond to the gyre's center, whose location varies throughout its evolution. The simulated daily evolution of the gyre velocity field in the near-surface layer during the September 2019 event is shown in Figure S2 in Supporting Information S1. Similar to Figure 4, the location of the gyre center and the associated pelagic upwelling follow the evolution of the gyre velocity field (Figure S3a in Supporting Information S1). Note that on 20 and 21 September, a cyclonic gyre in the east and anticyclonic gyre in the west of the *Grand Lac* are well developed. For details of this three-gyre pattern, see Hamze-Ziabari, Lemmin, et al. (2022).

3.3. Chimney-Like Pelagic Upwelling Observations During Weakly Stratified Seasons

During autumn and winter, colder air temperatures accompanied by stronger wind events erode the strong thermal stratification produced in the summer and move the thermocline downwards. As a result, the gyre velocity field can penetrate to greater depths, and thus can affect the strength and the depth of pelagic upwelling. To investigate the effect of seasonal changes, three field campaigns were carried out, each after a strong *Bise* event in October

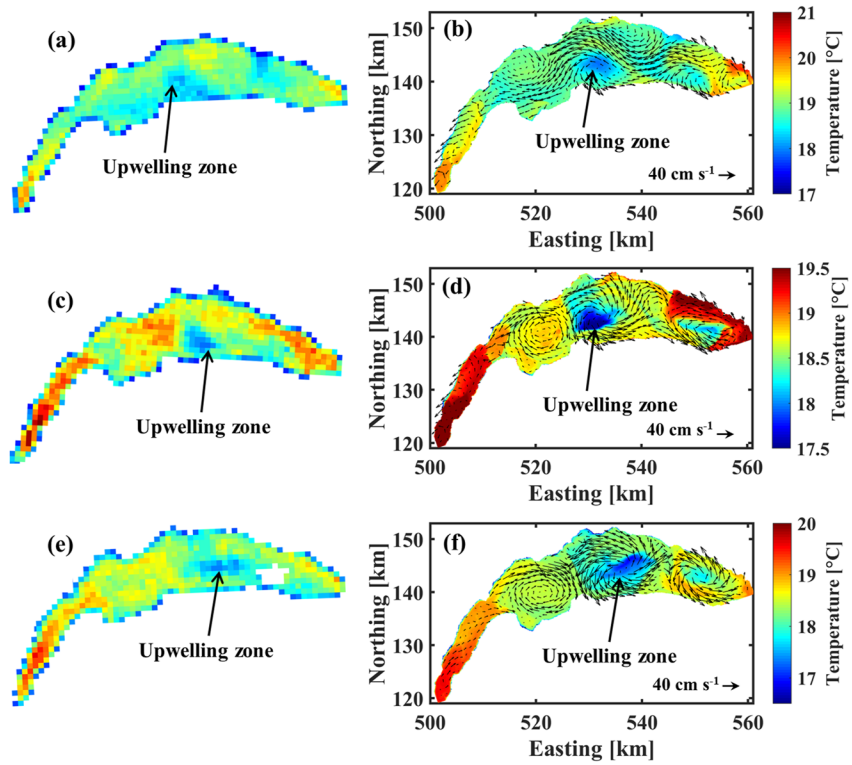

Figure 4. Left column: Advanced Very High-Resolution Radiometer (AVHRR) images. Right column: Corresponding simulated temperature (color contours) and near-surface velocity (black arrows) at 0.3 m depth. (a and b) 19 September 2019. (c and d) 20 September 2019. (e and f) 21 September 2019. Note that the AVHRR images and corresponding numerical results have identical colorbars.

2019 November 2019 and January 2020. The wind speed and direction for each event are shown in Figure S1 in Supporting Information S1. According to the numerical results, a cyclonic gyre is formed after each of these wind events (Figure 5), and the cold upwelling zone can again be seen near the lake surface, even though the thermocline is (much) deeper than in September 2019 (Figure 4). During these three field campaigns, the surface water temperatures at the center of the transects were, respectively, 0.4, 0.6, and 0.25°C lower than the ambient water temperature, and were equal to nearshore water temperatures at depths of ∼15, 25, and 70 m, measured at both ends of the transects. These observations suggest that these chimney-like upwelling events, which have not been reported before, are probably common features, and that their potential effect on different processes in lakes should be considered.

Despite the high spatial variability of the upwelling zone during the lifetime of a cyclonic gyre, model results and satellite imagery indicate that the pelagic upwelling can reach to the lake surface. Based on numerical results, the chimney-like pattern of dense water can persist for days to weeks. For example, the chimney-like upwelling lasted for almost 5 and 11 days, respectively, for the September 2019 and January 2020 events (Figures S2–S4 in Supporting Information S1). The occurrence and duration of chimney-like upwelling in the center of the lake are determined by the preceding and subsequent strong wind events. More details about the lifetime and the effect of wind on the September 2019 and January 2020 events are given in Text S1 and Figures S3 and S4 in Supporting Information S1.

3.4. Chimney-Like Upwelling Versus Submesoscale Filaments

Submesoscale cold filaments, that is, narrow bands of cold water in the near-surface layer, are ubiquitous inside cyclonic and anticyclonic gyres and eddies. The vertical structure of cold filaments appears as a column of well-mixed cold water in the epilimnion layer. For example, Hamze-Ziabari, Razmi, et al. (2022) showed that cold submesoscale filaments with a width ranging from 0.1 to 1 km can be formed at the edges and in the centers

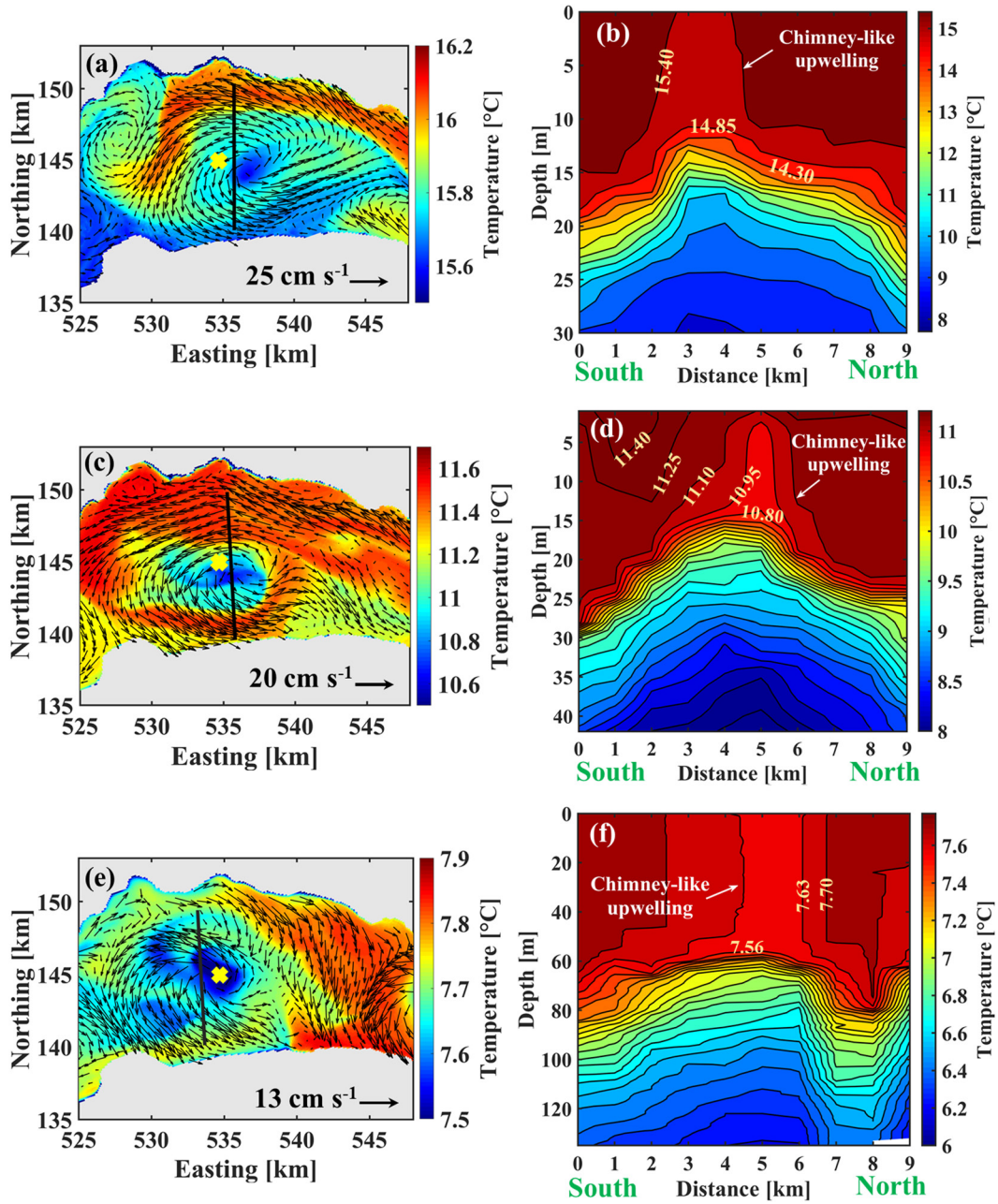

Figure 5. Left column: Numerical results of near-surface velocity (arrows) and temperature (colors) for the cyclonic gyre in the center of the *Grand Lac*. Right column: Field observations of chimney-like upwelling in the measured temperature profiles along transects (black lines in left panels) under weakly stratified conditions. (a and b) 25 October 2019. (c and d) 25 November 2019. (e and f) 27 January 2020. The yellow cross in the left panels indicates the location of the SHL2 station.

of the cyclonic gyres in Lake Geneva. It was suggested that the pelagic upwelling at the center of the lake provides the buoyancy gradient required for filamentogenesis or frontogenesis (Gula et al., 2014; McWilliams, 2019). A field campaign was conducted on 16 October 2021 after a strong *Bise* event in order to distinguish between submesoscale filaments and chimney-like upwelling. The spatial resolution of measurements was set at 300 m to capture submesoscale and mesoscale patterns within cyclonic gyres. The location of transect *T*, which consisted of 30 measurement points, was chosen based on the numerical forecast shown in Figure 6a.

The measured temperature profiles along transect *T* are plotted in Figure 6c. A dome-shaped thermocline and a chimney-like upwelling in the mixed layer were observed (Figures 6c and 6d). The chimney-like upwelling

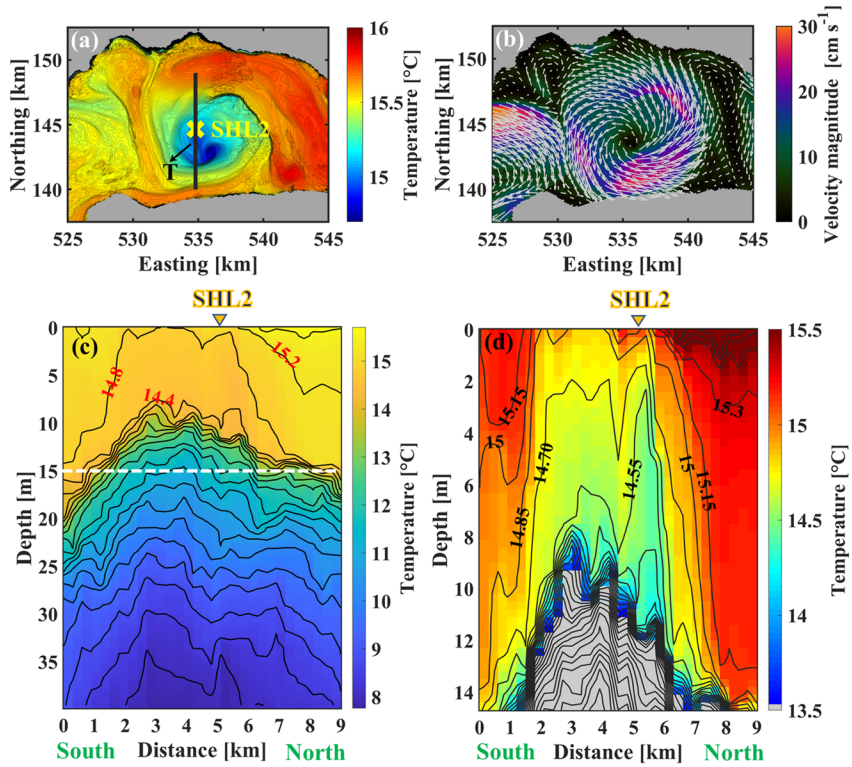

Figure 6. Numerical results of: (a) temperature and (b) velocity fields at 1-m depth for the cyclonic gyre in the center of the *Grand Lac* on 16 October 2022. The black line in (a) marks the predefined transect T (for the field campaign), which passes through station SHL2 (yellow cross). (c) Isotherm pattern obtained from temperature profiles measured along T showing the dome-shaped thermocline and the chimney-like pelagic upwelling. (d) Zoomed isotherm pattern (area above horizontal white-dashed line in panel c) of temperature profiles in the epilimnion layer measured along T. Note the cold filament between 5 and 6 km in (d). The location of monitoring station SHL2 is indicated on top of panels (c and d). Colorbars give the range of the parameters.

structure has a width of nearly 4 km, which is much wider than that of submesoscale filaments reported in the literature. On the other hand, a smaller cold structure (between 5 and 6 km distance in Figure 6d) with a width of less than 1 km is observed near the upwelling zone. A combination of the buoyancy gradient generated by a chimney-like upwelling and the background straining flow field can lead to the isolation and elongation of such filamentary patterns in the center of cyclonic circulations. Thus, a chimney-like upwelling in the mixed layer is required for filament formation in the center of the gyre. Its formation mechanism, however, is different than that of filamentogenesis/frontogenesis. Transect *T* passes through the location of CIPEL monitoring station SHL2 (see Figure 1 for location), where long-term data of different physical and biological parameters are collected. From Figure 6c, it is evident that measurements taken at SHL2 are affected by the pelagic upwelling as will be further discussed below.

4. Discussion

This study, carried out in Lake Geneva, makes evident for the first time in a lake that intense pelagic upwelling occurs in the center of a basin-scale cyclonic gyre. It was shown that cold water that upwelled from the thermocline layer frequently reached up to the surface, as confirmed by satellite images. Detailed field measurement campaigns confirm the existence of a dome-shaped thermocline and the gyre current pattern that causes this chimney-like upwelling to rise like a cylindric vertical water column, as predicted by theory. 3D numerical modeling results agree with these observations. Based on 3D numerical modeling results, we discuss below the processes that can or cannot cause and modify pelagic upwelling. Furthermore, we will assess the effects of pelagic upwelling on biogeophysical processes and how their long-term monitoring at a fixed location and their quantification based on these measurements may be affected by the presence of a pelagic upwelling zone.

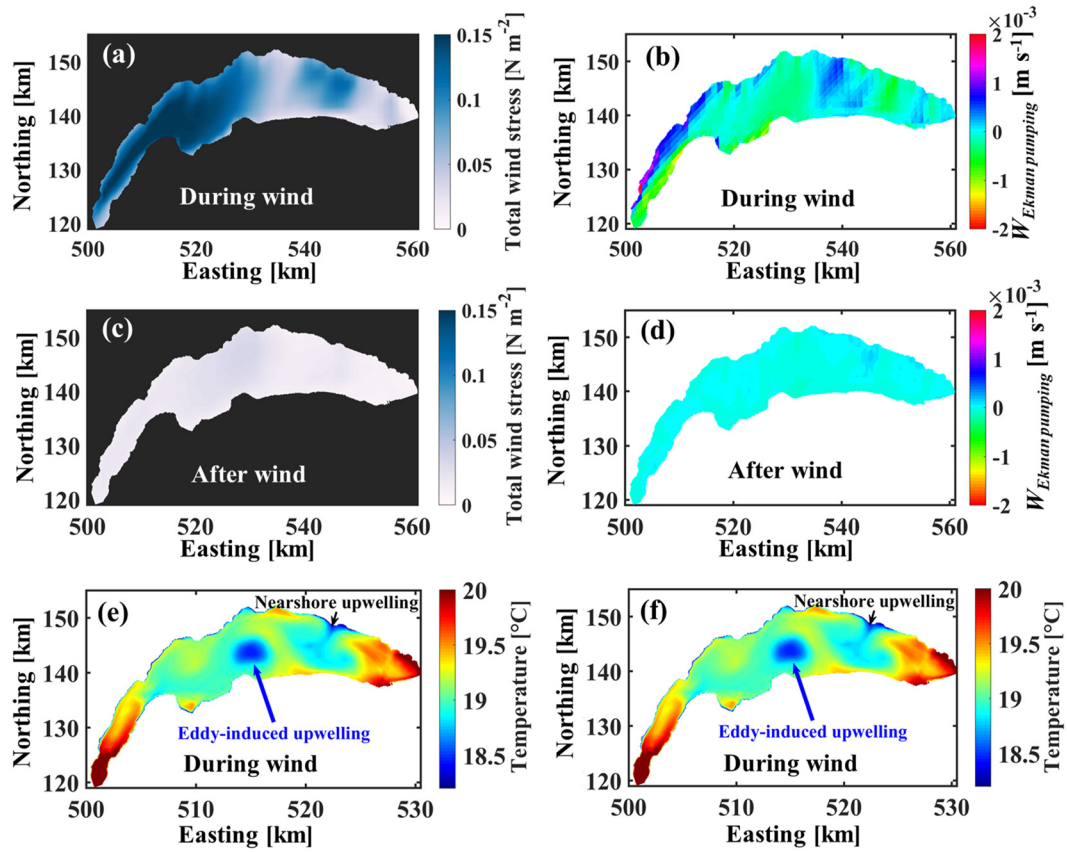

Figure 7. The *Bise* wind event that lasted from 18–20 September 2019 and its effects. (a) Average wind stress and (b) estimated Ekman pumping velocity ($W_{\text{Ekman pumping}}$) during the *Bise* event. (c) Average wind stress and (d) estimated Ekman pumping velocity after the *Bise* event. Daily average temperature in the near-surface layer (e) at 0.3 m depth and (f) at 15 m depth during the *Bise* event. The colorbars indicate the range of the parameters.

4.1. Cause of Upwelling

4.1.1. Ekman Pumping

Ocean studies indicate that cyclonic winds can cause divergence of Ekman mass transport in offshore areas, resulting in pelagic upwelling. For example, Lu et al. (2020) theoretically demonstrated how TC can cause vertical perturbations of background cyclonic and anticyclonic circulations. They showed that geostrophic responses to TC forcing can be divided into three layers: (a) the Ekman layer, (b) an expansionary layer, and (c) a contractive layer. In the Ekman layer, a TC produces a chimney-like upwelling, accompanied by an expansionary upwelling zone in the thermocline layer and, as depth increases, the Ekman pumping decays. Although Ekman pumping was proposed as a mechanism responsible for pelagic upwelling in that study, there is little field evidence of its role in large lakes.

To understand the mechanism behind the observed chimney-like upwelling in Lake Geneva, we first investigated the possibility of Ekman pumping based on numerical simulations driven by COSMO wind data. Using daily averaged wind stresses derived from COSMO, the Ekman pumping velocities (Equation 3) were calculated during and after the *Bise* event on September 2019 (Figures 1b and 7). Figures 7e and 7f display the daily average water temperature in the near-surface layer and, at a depth of 15 m, respectively, during the *Bise* event. Two distinct cold-water zones are evident in the near-surface layers: (a) nearshore upwelling, and (b) gyre/eddy-induced upwelling. A similar nearshore upwelling pattern in the same area is also seen in the AVHRR data (see Figure 4a). Nearshore upwelling was previously observed in Lake Geneva (Reiss et al., 2020). Comparing Figures 7e and 7f with Figures 7a, 7b, and 7d, it is evident that the offshore Ekman pumping velocity resulting from wind stress curl is small and negative and did not cause the eddy-induced cold-water pelagic upwelling zones in the center of the lake. Ekman pumping can therefore be ruled out as the driver of the chimney-like upwelling in the center of Lake Geneva.

4.1.2. Nonlinear Dynamics Associated With a Cyclonic Gyre

In order to investigate the dynamics of the gyre flow field in more detail, the effects of the different terms in the momentum equation are considered. For this, the vertically averaged horizontal momentum equation over the depth layers influenced by the gyre velocity field (i.e., the thermocline layer and epilimnion) is expressed as (Brett, 2018; Brett et al., 2020; Cimatoribus et al., 2018; Vallis, 2017):

$$\frac{\partial \boldsymbol{U}_h}{\partial t} = \boldsymbol{P} + \boldsymbol{N} + \boldsymbol{C} + \boldsymbol{F} - \boldsymbol{D} \tag{6}$$

where $\boldsymbol{U_h} = (u,v)$ is the horizontal velocity field, $\boldsymbol{P} = \left(-\frac{1}{\rho}\frac{\partial P}{\partial x}, -\frac{1}{\rho}\frac{\partial P}{\partial y}\right)$ is the acceleration induced by the barotropic and baroclinic pressure gradients, $\boldsymbol{N} = \left(-\left(\vec{\boldsymbol{u}}.\nabla\right)u, -\left(\vec{\boldsymbol{u}}.\nabla\right)v\right)$ is the acceleration caused by the nonlinear (advection) terms, $\boldsymbol{C} = (fv, -fu)$ is the acceleration caused by the Coriolis effect, $\boldsymbol{F} = (F_x,F_y)$ is the acceleration induced by external forces, and $\boldsymbol{D} = (-\nu\nabla^2 u, -\nu\nabla^2 v)$ is the deceleration due to dissipation (i.e., bulk, lateral, and bottom friction). $\vec{\boldsymbol{u}}$ is the three-dimensional velocity vector, ν is viscosity, ρ is density, and t is time. First, the mean zonal and meridional momentum trends caused by each term in the equation are determined for the full lifetime of the gyre. The averaged spatial variability during the lifetime of a cyclonic gyre in magnitude and the direction of the momentum trends induced by the different terms are then examined. This analysis is carried out for the September 2019 event for which details of the dynamics are shown above (Figures 1c, and 2–4).

The vertically (over ~30 m) and temporally (~6 d) averaged horizontal momentum trends of the different terms in Equation 6 for the cyclonic gyre that developed during the September 2019 event are illustrated in Figure 8. The resultant horizontal momentum acceleration trend, that is, the left-hand side of Equation 6, indicates a divergent pattern, as expected for a cyclonic gyre in the Northern Hemisphere (Figure 8a). In the southern part of the gyre, the horizontal acceleration is much greater compared to its northern part. This total acceleration is compared to the contribution of each of the right-hand side terms in Equation 6 in the remaining panels of Figure 8. According to Figures 8b and 8c, the Coriolis and pressure terms act in opposite directions. In the cyclonic gyre in the center of the *Grand Lac* basin, the Coriolis term shows a divergent pattern, and the pressure term, a convergent pattern. The pressure effect is slightly greater than the Coriolis effect, but is of the same order. The pressure term is the only term that opposes the advective term (Figure 8a). These two terms clearly cannot be responsible for the resultant momentum acceleration pattern in terms of direction and magnitude. The external forcing term (Figure 8d) is considerably less important than the Coriolis and pressure terms. Furthermore, there is no correlation between the patterns of local atmospheric forcing and the resultant acceleration. The dissipation term (Figure 8f) is negligible compared to the other terms and is only important in the nearshore zones. The nonlinear (advective, Figure 8e) term, however, exceeds the effect of all the other terms. It is of the same order as the resultant momentum acceleration (Figure 8a), but slightly greater, compensated in part by the pressure term. These results are in agreement with the findings by Bohle-Carbonell and Lemmin (1988), who showed that the nonlinear acceleration terms computed for Lake Geneva could be as large or greater than the other terms. Thus, this nonlinear divergent nature of gyre dynamics can be responsible for the formation of the observed intense chimney-like upwelling at its center. The heterogeneous divergent flow shown in Figure 8a may also result in considerable horizontal strain in the gyre's center and around its periphery.

4.1.3. Ageostrophic Divergence and Strain

Numerical results and AVHRR data (Figures 2 and 4) indicate that the gyre velocity field continuously changes as it develops, and the upwelling zone changes accordingly. Moreover, as shown in Figure 8, the nonlinear divergence dynamics associated with the gyre flow field can be spatially variable. In contrast to the ocean, a lake gyre velocity field is strongly affected by the morphology of its basin. For example, in long narrow lakes, such as Lake Geneva, there is a tendency for the gyre velocity field and the associated pelagic upwelling zone to form an elliptical pattern (e.g., Figure 2a). Furthermore, local winds and interactions with other large-scale currents can alter the gyre velocity field. Due to sudden changes in the gyre velocity field, divergence and strain fields within the gyre can be spatially variable.

A simplified conceptual diagram of the inward and outward distortions that can be caused by an elliptical velocity field is presented in Figures 9a and 9b. Conservation of mass dictates that an inward distortion along the minor axis of the ellipse leads to flow convergence. On the other hand, an outward distortion leads to flow divergence along the major axis. The center of a gyre can be subjected to high strain as a result of both inward and outward

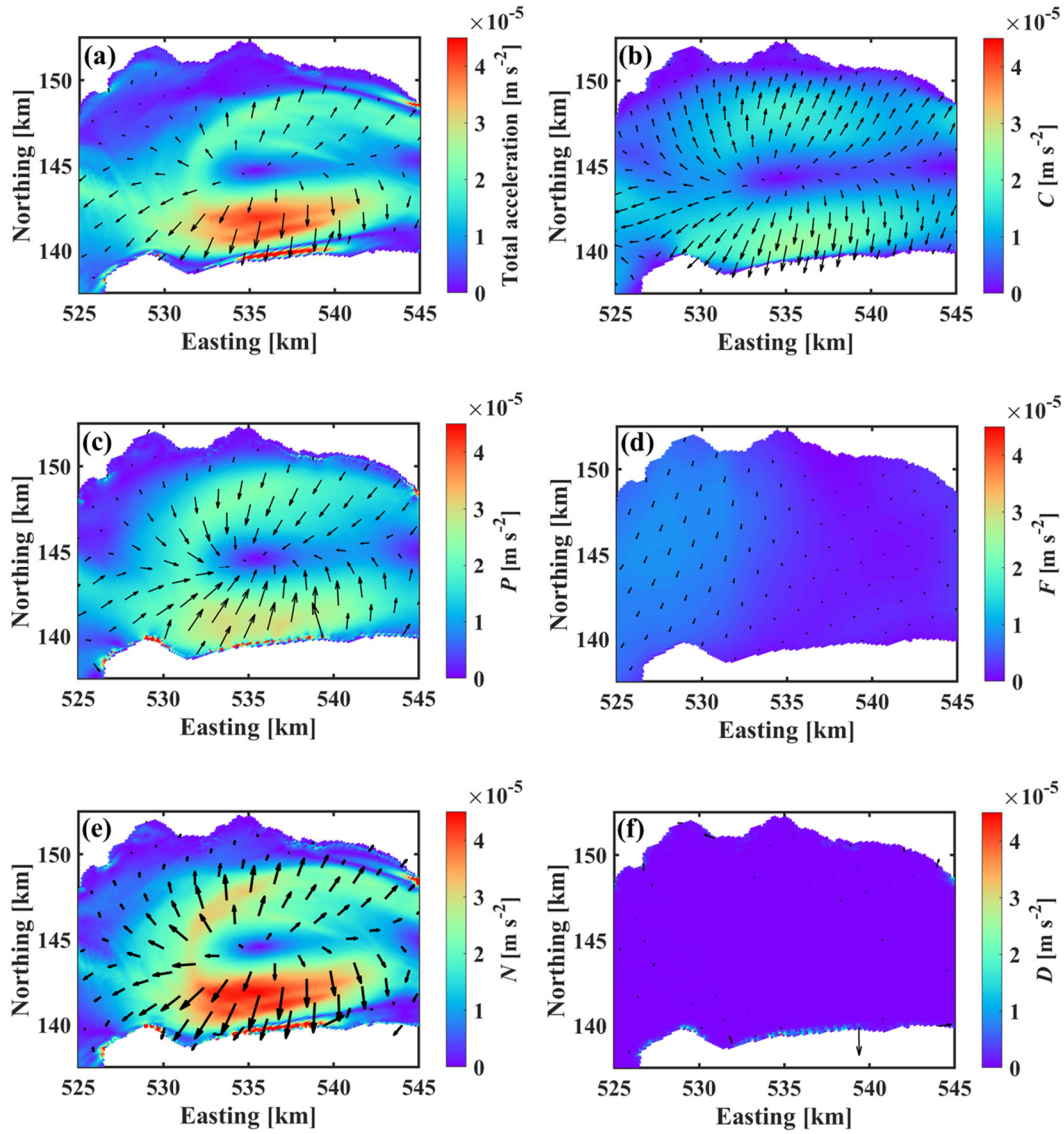

Figure 8. The contribution of different terms to the vertically (30 m) and temporally (6 d) averaged horizontal momentum equation for the September 2019 *Bise* wind event (Figure 1b), computed using Equation 6. (a) Total acceleration, (b) Coriolis term, (c) pressure term, (d) external forcing, (e) nonlinear (advective) term, and (f) dissipative term. Orientation and length of the arrows indicate the direction and intensity, respectively, of the trend. Colorbars give the range of parameters.

distortions. As an example, the horizontal divergence parameter σ (Figures 9e and 9f) and the magnitude of horizontal strain rate S (Figures 9g and 9h) are shown for the September 2019 *Bise* event and are defined as (Gula et al., 2014; McWilliams, 2019):

$$\sigma = u_x + v_y \tag{7}$$

$$S = \sqrt{(u_x - v_y)^2 + (v_x + u_y)^2} \tag{8}$$

with u and v being the east and the north components, respectively, of the velocity vector. The corresponding upwelling patterns are quite different (Figures 9c and 9d). In general, flow divergence dominates the cyclonic gyre's velocity field. However, the sign of the divergence parameter can change at the edges and in the center of the gyre, due to the interaction with basin borders and other large-scale currents, and the constant distortions of the gyre's velocity field. According to Figures 9g and 9h, the distortion of the gyre velocity field results in a high horizontal strain rate inside the cyclonic gyre. It can be observed that the pelagic upwelling area is generally

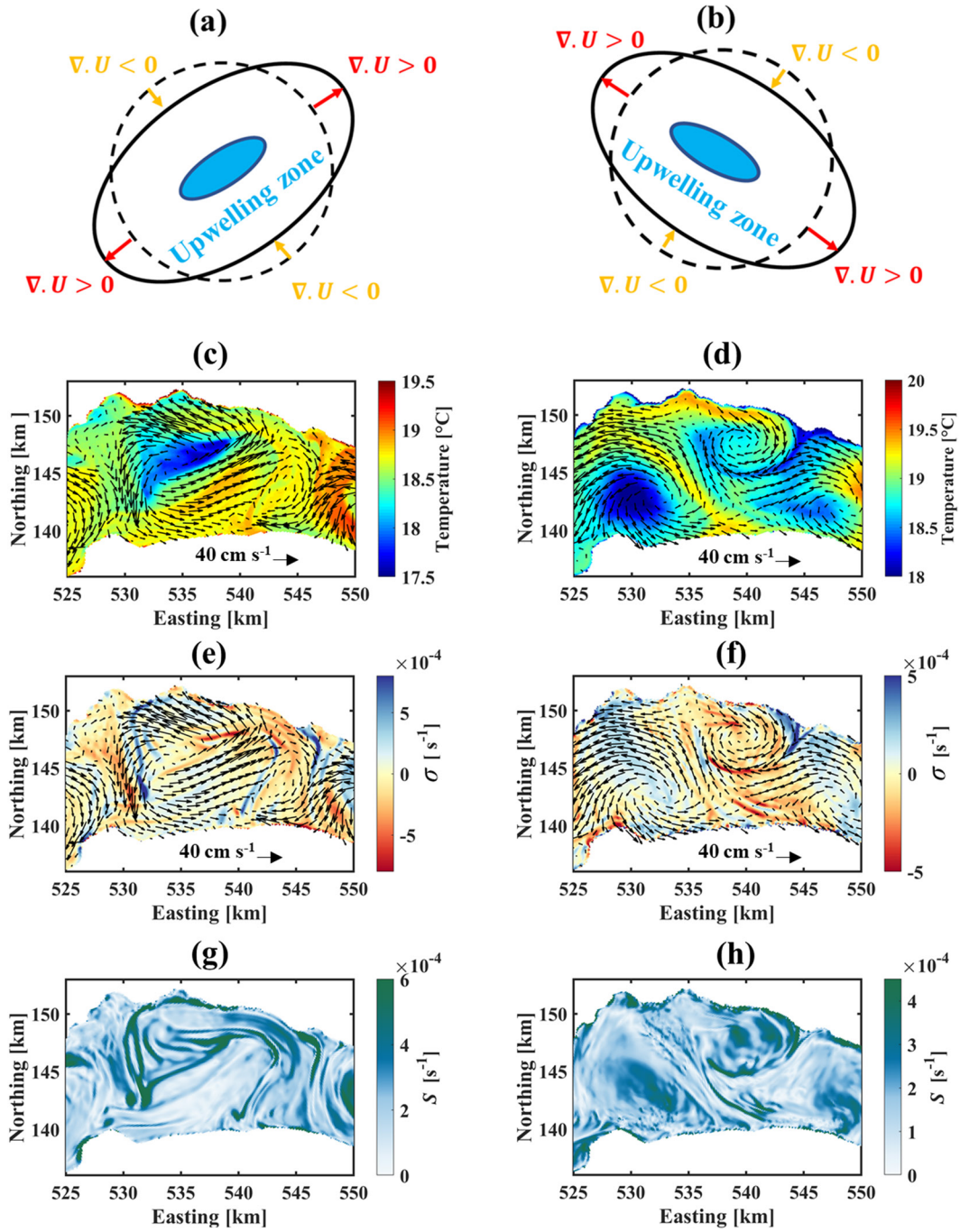

Figure 9. Two different velocity fields during the September 2019 *Bise* wind event caused by inward (left column) and outward distortion (right column). (a and b) Schematic view of inward and outward distortion in an elliptical velocity field. (c) and (d) Simulated temperature at 2-m depth. (e and f) Computed divergence parameter. (g and h) Computed horizontal strain rate, *S*. Colorbars give range of parameters. Black arrows indicate the near-surface velocity fields.

associated with high strain zones, and its shape is similar to that of the horizontal strain rate. There are, however, some areas of high strain that are not associated with cold water, such as the nearshore areas and the edges of the gyre where it interacts with other large-scale currents. Pelagic upwelling caused by gyres is therefore a 3D process, which cannot be studied solely on the basis of horizontal patterns of divergence and strain parameters.

The effects of heterogeneous divergence or convergence within the gyre flow field as well as the strain caused by it were further investigated for the October, November, and January field measurement campaigns along

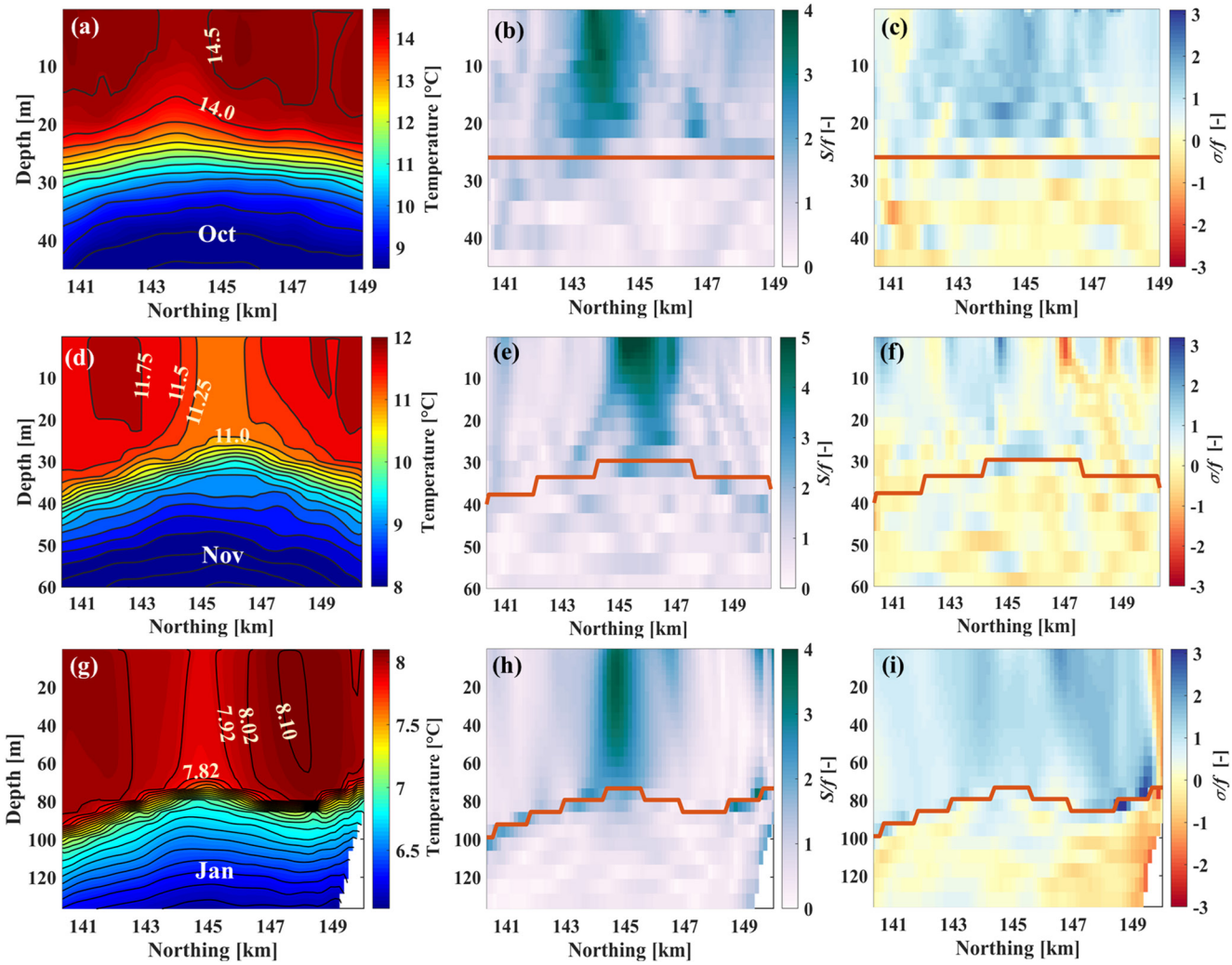

Figure 10. Simulated profiles of temperature (left column), horizontal strain rate (center column), and divergence parameters (right column) along the transects shown in Figure 5 for the (a–c) October 2019, (d–f) November 2019, and (g–i) January 2020 field campaigns. Colorbars give the range of the parameters. The red line indicates the zone of maximum stratification strength. Note that temperature ranges are different in (a, d, and g).

three transects (see Figure 5 for transect locations), where chimney-like upwelling was detected (Figure 10). The chimney-like upwelling patterns observed in the field and the corresponding simulations are in good agreement (Figures 5 and 10). The divergence parameter indicates that the flow generally diverges in the mixed layer, whereas it converges in the deeper layers below the zone of maximum stratification strength (red horizontal lines in Figure 10). It appears that there is no direct correlation between the chimney-like upwelling in the mixed layer and the flow divergence in the epilimnion. A high ageostrophic strain (>f, the Coriolis frequency) zone is found in the epilimnion at the location where chimney-like upwellings were observed (Figure 10). The higher strain rate extends from the near-surface down to the thermocline layer and potentially stimulates ageostrophic perturbations (see Figure S5 in Supporting Information S1 as an example of the hourly evolution of strain rate and chimney-like upwelling). The perturbed cold thermocline water can be transported by the background divergence flow into the epilimnion. This results in an upward flux of cold water from the thermocline layer, which is followed by a chimney-like pelagic upwelling depending on the shape of the area imposed by the strain. Such strong 3D ageostrophic strain accompanied by upwelling can increase the ageostrophic kinetic energy, favor a higher chlorophyll growth rate, and enhance primary production (Zhang et al., 2019).

Several physical processes, such as lateral stirring, advection by the rotational velocity of gyres or eddies, and the translation of the gyre velocity field, can continuously alter the shape of the chimney of cold upwelled water in different depth layers (Lv et al., 2022). The gyre velocity is almost uniformly distributed in the deeper layers (e.g.,

15-m depth) and the upwelling appears as a well-defined circular cold pattern (Figure 11). On the other hand, the gyre velocity field is spatially variable in the near-surface layers, primarily due to its nonlinear dynamics and the constantly changing local atmospheric forcing conditions. Upwelling patterns, therefore, can differ considerably in different depth layers (Figure 11). In AVHRR images, cold areas are the superposition of upwelling patterns and other local physical processes. AVHRR data on 21 September (Figure 4e), which correspond to the pelagic upwelling shown in Figure 11, may therefore underestimate the area affected by the pelagic upwelling, in part due to limited resolution.

4.2. Effect of Thermocline Shape on Long-Term Observations at a Fixed Monitoring Station

There is growing concern about the widespread reliance on a single or a few profile measurements for monitoring and quantifying different processes in large lakes (Gaillard et al., 2022). Vertical upward transport of thermocline water can have a significant impact on physical and biological processes of a lake. A field study conducted in Lake Issyk-Kul revealed that the dissolved oxygen level in the near surface layers of the pelagic upwelling zone can increase (Romanovsky & Shabunin, 2002). In Lake Tanganyika, an increase in nutrient concentrations and phytoplankton chlorophyll levels were found in pelagic upwelling zones (Corman et al., 2010). Primary production in upwelling areas is expected to increase as the nutrient load increases (Jane et al., 2021).

Long-term profile measurements taken at monitoring station SHL2 (Figure 1) in Lake Geneva, for example, are used by CIPEL to quantify various physical and biological processes in budget estimates to determine long-term water quality development in the whole lake (e.g., CIPEL, 2018). The above numerical results and field observations show that station SHL2 is often located in the pelagic upwelling zone of the cyclonic gyre in the center of the *Grand Lac* basin (e.g., Figures 5 and 6). Thus, measurements taken at that station may be affected by pelagic upwelling dynamics.

To determine the structure of pelagic upwelling over a longer period, EOF analysis can be used to compute the dominant spatial temperature variability. In EOF analysis, the signature of upwelling/downwelling induced by cyclonic/anticyclonic circulations can appear as nearly circular areas with temperatures that are different than the surrounding waters. Since the signature of upwelling is more obvious in deeper layers and it is less regular near the surface due to the high spatial variability of the upwelling zone and local external forces (Figure 11), the EOF analysis was performed on the average temperature of the thermocline layer (Figure 12). The average temperature of the thermocline layer was calculated hourly, resulting in approximately 720 numerical snapshots for each month. These hourly averages are used for each computation of the EOF analysis. For each month, the depth of the thermocline layer was determined following Xu et al. (2019). The results of the EOF analysis show that pelagic upwelling can be identified by a circular cold-water area in the center of the lake in all months (Figure 12). With the exception of August and November 2019, the upwelling signature appears in the first mode. It is plausible that pelagic upwelling, which lasts for several days to weeks depending on wind events, could contribute to the spatial variability of temperature in the thermocline layer at station SHL2. Figure 12 shows the corresponding principal component time series of EOF modes for different months. The spatial anomalies are monthly and seasonally variable and may depend on the change of gyre rotational signs after *Bise* and *Vent* wind events (Figure 1). As expected, the amplitude of these spatial anomalies gradually decreases from September to January due to the weakening of the thermocline. This could lead to a reduction in the magnitude of the spatial variability of water temperature in the thermocline. To investigate the temporal variability of water temperature at SHL2 induced by pelagic upwelling, simulation results were combined with field observations (Text S2 and Figure S6 in Supporting Information S1).

During the study period from 1 June 2019–1 January 2020, pelagic upwelling modified the temperature profile at the SHL2 location 41.5% of the time (101.5 out of 245 days). Simulated temperature profiles at the SHL2 location indicate that during this period, five out of 12 SHL2 profiles may have been affected by pelagic upwelling caused by cyclonic gyres generated by strong *Bise* events (Figure S6 and Text S2 in Supporting Information S1). Thus, care should be taken when developing long-term concepts based solely on SHL2 measurements. Further research is needed to determine the impact of pelagic upwelling on biological and chemical parameters and on water quality in order to quantify the effect of pelagic upwelling on biogeochemical processes and on measurements taken at single, fixed monitoring stations.

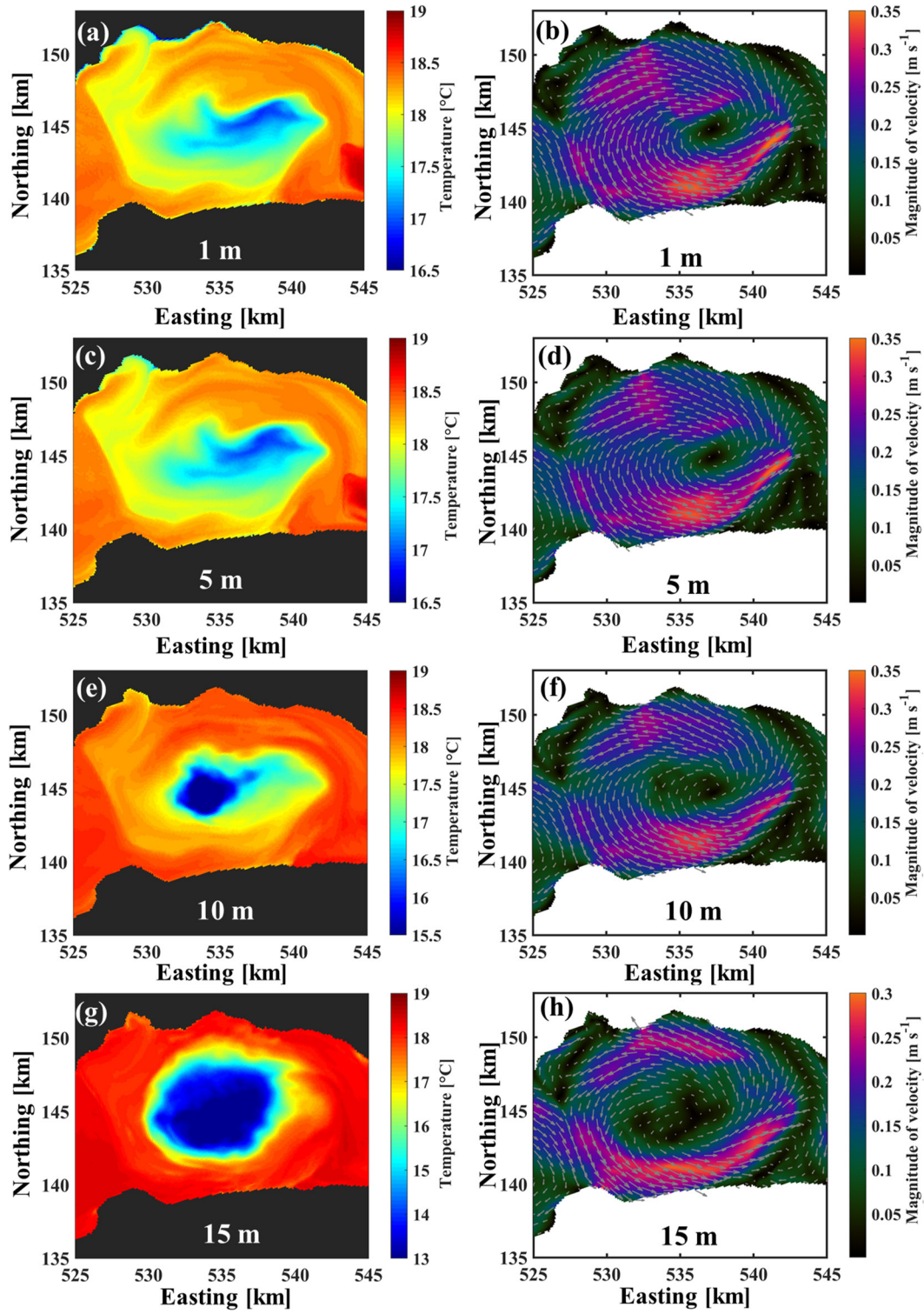

Figure 11. Left column: Modeled distributions of temperature (indicating pelagic upwelling). Right column: Gyre velocity field (a–h) Temperature and velocity fields at the indicated depths in the large-scale cyclonic gyre in the center of the *Grand Lac* for 21 September 2019. Colorbars indicate the range of the parameters. Note that the temperature ranges in the left panels change. Arrows in right panels give the velocity vector orientation.

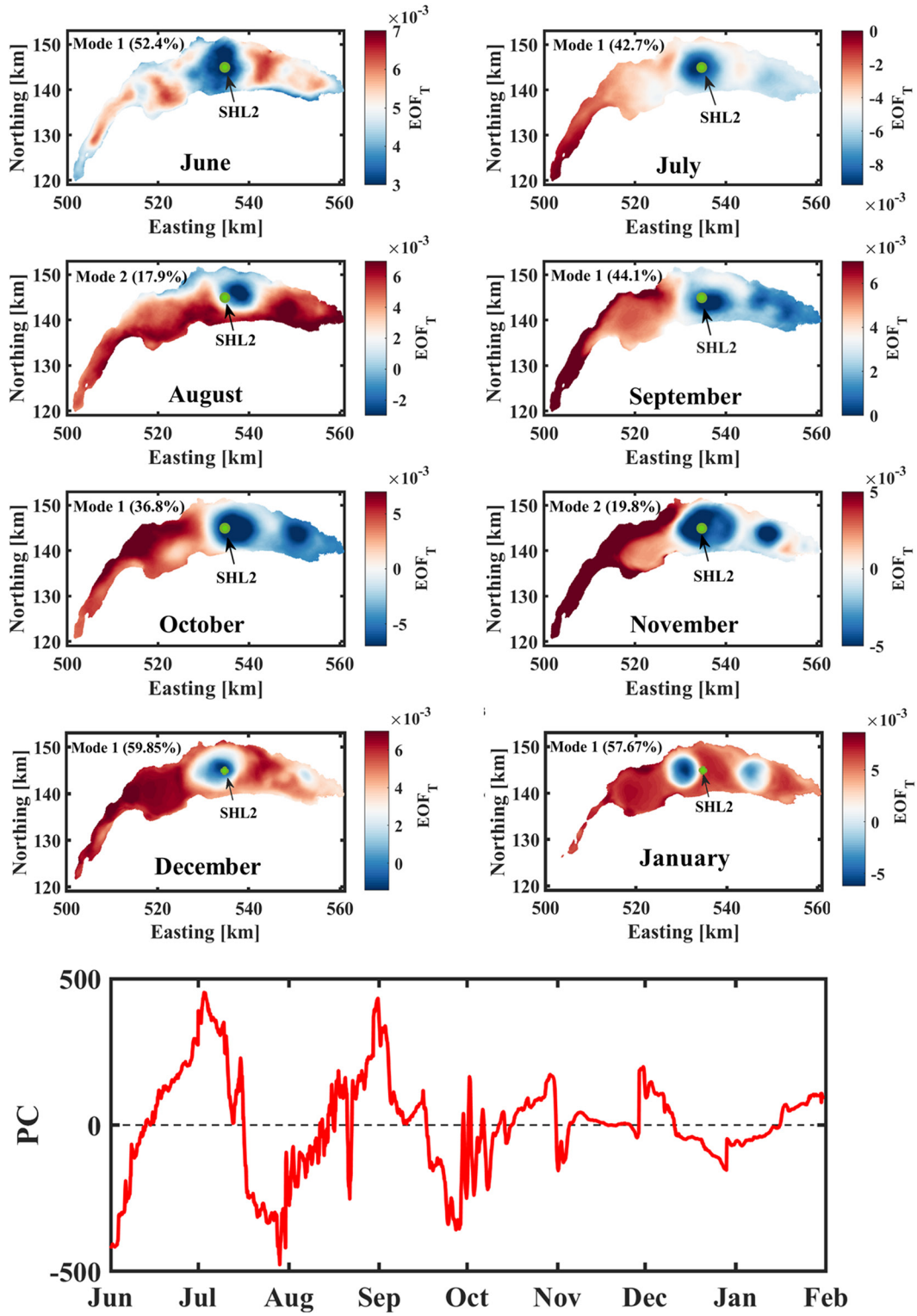

Figure 12. Empirical Orthogonal Function (EOF) analysis of the average temperature (*T*) in the thermocline layer for different months from June 2019 to January 2020; the month and the dominant mode (% of occurrence) are indicated in each panel. The green circle marks the location of station SHL2 that most of the time is in the large-scale (dark blue) gyre area where pelagic upwelling occurs in the *Grand Lac*. The bottom panel shows the principal component of the EOFs for different months.

5. Summary and Conclusions

A unique combination of field measurements, 3D modeling, and satellite imagery allowed documenting for the first time in a lake (Lake Geneva) the frequent occurrence of dome-shaped thermoclines and strong pelagic upwelling in the center of cyclonic basin-scale gyres under different stratification conditions. Field measurement campaigns were designed based on hydrodynamic modeling to capture pelagic upwelling in the presence of a shallow, strong or a deep, weak thermocline. It was shown that.

- Pelagic upwelling forms chimney-like structures that can transport cold thermocline water upwards to the epilimnion layer and frequently even to the lake surface as confirmed in thermal (AVHRR) imagery and numerical simulations.
- The height of the chimney-like structure was about 10–20 m in September 2019 (shallow, strong thermocline) and 60–80 m in January 2020 (deep, weak thermocline).
- According to the modeling results, the detected upwelling can persist for 5–11 days depending on preceding and subsequent wind conditions.
- Neither the presence of wind stress over cyclonic circulations, nor wind stress curl was observed in the upwelling zone during and after wind events. Numerical results indicate that Ekman pumping is not be responsible for the formation of this chimney-like upwelling; Instead, it is the 3D ageostrophic strain field which is caused by gyre distortion.
- The contribution of the terms of the momentum equation, vertically averaged over the lifetime of a gyre, revealed that the nonlinear term is the dominant acceleration term. A heterogeneous divergence flow formed around the pelagic upwelling zone due to the influence of the advective acceleration.
- The heterogenous divergence flow associated with the gyre flow field and the continuous distortion of the gyre during its evolution produce an ageostrophic strain in the center of the cyclonic gyre that can penetrate the thermocline layer, even a deep thermocline (~60–80 m).
- Cold water was transported from the thermocline to the mixed layer and to the water surface by the background divergence flow in the epilimnion layer. The cold-water areas observed in the AVHRR images correspond to the areas affected by the chimney-like upwelling; their shape is mainly determined by the horizontal strain field at the water surface.

Since large (basin-scale) cyclonic gyres are ubiquitous in Lake Geneva and other large lakes, and the underlying concepts of our analysis are universal, the findings about chimney-like pelagic upwelling can be applied to other large lakes. This suggests that these newly discovered chimney-like pelagic upwelling events occur regularly and thus can affect the interplay of complex 3D biochemical and physical processes occurring in lakes. Intense pelagic upwelling may, for example, impact on phytoplankton growth cycles due to the vertical redistribution of nutrients and potential pollutants. It can also affect routine single profile measurements taken at a fixed station, if the station is located within the pelagic upwelling zone. Since long-term monitoring measurements at fixed locations are frequently used to evaluate the water quality status of the entire lake, the effect of pelagic upwelling can have severe consequences if lake management concepts are solely based on these measurements. Therefore, the interplay of physical, biological and chemical processes within gyres and pelagic upwelling should be taken into consideration.

Acknowledgments
This research was supported by the Swiss National Science Foundation (SNSF Grant 178866). The spatiotemporal meteorological data were provided by the Federal Office of Meteorology and Climatology in Switzerland (MeteoSwiss). We thank the Commission Internationale pour la Protection des Eaux du Léman (CIPEL) for in situ temperature measurements. Water temperature profiles were collected at the CIPEL SHL2 station for 2018–2019 by the Eco-Informatics ORE INRA Team at the French National Institute for Agricultural Research (SOEREOLA-IS, INRA Thonon-les-Bains, France). Open access funding provided by Ecole Polytechnique Federale de Lausanne.

Data Availability Statement

The three-dimensional model used in this study is based on the MIT General Circulation Model (MITgcm), which is publicly available at Campin et al. (2021). All data used in the paper are available from https://zenodo.org/record/7941268#.ZGOJtaVBxPY (Hamze-Ziabari et al., 2023).

References

Akitomo, K., Tanaka, K., Kumagai, M., & Jiao, C. (2009). Annual cycle of circulations in Lake Biwa, part 1: Model validation. *Limnology*, *10*(2), 105–118. https://doi.org/10.1007/s10201-009-0267-7

Bauer, S. W., Graf, W. H., Mortimer, C. H., & Perrinjaquet, C. (1981). Inertial motion in Lake Geneva (Le Léman). *Archives for Meteorology, Geophysics and Bioclimatology. Series A: Meteorology and Atmospheric Physics*, *30*(3), 289–312. https://doi.org/10.1007/BF02257850

Beletsky, D., Hawley, N., & Rao, Y. R. (2013). Modeling summer circulation and thermal structure of Lake Erie. *Journal of Geophysical Research: Oceans*, *118*(11), 6238–6252. https://doi.org/10.1002/2013JC008854

Beletsky, D., Hawley, N., Rao, Y. R., Vanderploeg, H. A., Beletsky, R., Schwab, D. J., & Ruberg, S. A. (2012). Summer thermal structure and anticyclonic circulation of Lake Erie. *Geophysical Research Letters*, *39*(6), L06605. https://doi.org/10.1029/2012GL051002

Beletsky, D., Saylor, J. H., & Schwab, D. J. (1999). Mean circulation in the Great Lakes. *Journal of Great Lakes Research*, *25*(1), 78–93. https://doi.org/10.1016/S0380-1330(99)70718-5

Beletsky, D., & Schwab, D. (2008). Climatological circulation in Lake Michigan. *Geophysical Research Letters*, *35*(21), L21604. https://doi.org/10.1029/2008GL035773

Bennington, V., McKinley, G. A., Kimura, N., & Wu, C. H. (2010). General circulation of Lake Superior: Mean, variability, and trends from 1979 to 2006. *Journal of Geophysical Research*, *115*(C12), C12015. https://doi.org/10.1029/2010JC006261

Bohle-Carbonell, M., & Lemmin, U. (1988). Observations on non-linear current fields in the Lake of Geneva. *Annales Geophysicae*, *6*(1), 89–100.

Bouffard, D., Kiefer, I., Wüest, A., Wunderle, S., & Odermatt, D. (2018). Are surface temperature and chlorophyll in a large deep lake related? An analysis based on satellite observations in synergy with hydrodynamic modelling and in-situ data. *Remote Sensing of Environment*, *209*, 510–523. https://doi.org/10.1016/j.rse.2018.02.056

Brannigan, L. (2016). Intense submesoscale upwelling in anticyclonic eddies. *Geophysical Research Letters*, *43*(7), 3360–3369. https://doi.org/10.1002/2016GL067926

Bravo, L., Ramos, M., Astudillo, O., Dewitte, B., & Goubanova, K. (2016). Seasonal variability of the Ekman transport and pumping in the upwelling system off central-northern Chile (∼30° S) based on a high-resolution atmospheric regional model (WRF). *Ocean Science*, *12*(5), 1049–1065. https://doi.org/10.5194/os-12-1049-2016

Brett, G. E. (2018). *Chaotic advection, mixing, and property exchange in three-dimensional ocean eddies and gyres*. Doctoral dissertation, Massachusetts Institute of Technology. Retrieved from http://hdl.handle.net/1721.1/117913

Brett, G. J., Pratt, L. J., Rypina, I. I., & Sánchez-Garrido, J. C. (2020). The Western Alboran Gyre: An analysis of its properties and its exchange with surrounding water. *Journal of Physical Oceanography*, *50*(12), 3379–3402. https://doi.org/10.1175/JPO-D-20-0028.1

Campin, J. M., Heimbach, P., Losch, M., Forget, G., edhill3 Adcroft, A., amolod Menemenlis, D., et al. (2021). MITgcm/MITgcm: checkpoint67z (Version checkpoint67z) [Software]. Zenodo. https://doi.org/10.5281/zenodo.4968496

Cimatoribus, A. A., Lemmin, U., & Barry, D. A. (2019). Tracking Lagrangian transport in Lake Geneva: A 3D numerical modeling investigation. *Limnology & Oceanography*, *64*(3), 1252–1269. https://doi.org/10.1002/lno.11111

Cimatoribus, A. A., Lemmin, U., Bouffard, D., & Barry, D. A. (2018). Nonlinear dynamics of the nearshore boundary layer of a large lake (Lake Geneva). *Journal of Geophysical Research: Oceans*, *123*(2), 1016–1031. https://doi.org/10.1002/2017JC013531

CIPEL. (2018). Rapports sur les études et recherches entreprises dans le bassin lémanique, Campagne 2017. Commission internationale pour la protection des eaux du Léman (CIPEL), Nyon, Switzerland. Retrieved from http://www.cipel.org/wp-content/uploads/2018/04/RapportScientifique_camp_2016_VF.pdf

Corman, J. R., McIntyre, P. B., Kuboja, B., Mbemba, W., Fink, D., Wheeler, C. W., et al. (2010). Upwelling couples chemical and biological dynamics across the littoral and pelagic zones of Lake Tanganyika, East Africa. *Limnology & Oceanography*, *55*(1), 214–224. https://doi.org/10.4319/lo.2010.55.1.0214

Csanady, G. T. (1968). Wind-driven summer circulation in the Great Lakes. *Journal of Geophysical Research*, *73*(8), 2579–2589. https://doi.org/10.1029/JB073i008p02579

Csanady, G. T. (1973). Wind-induced barotropic motions in long lakes. *Journal of Physical Oceanography*, *3*(4), 429–438. https://doi.org/10.1175/1520-0485(1973)003<0429:WIBMIL>2.0.CO;2

Csanady, G. T. (1977). On the cyclonic mean circulation of large lakes. *Proceedings of the National Academy of Sciences U.S.A.*, *74*(6), 2204–2208. https://doi.org/10.1073/pnas.74.6.2204

Endoh, S., Watanabe, M., Nagata, H., Maruo, F., Kawae, T., Iguchi, C., & Okumura, Y. (1995). Wind fields over Lake Biwa and their effect on water circulation. *Japanese Journal of Limnology*, *56*(4), 269–278. https://doi.org/10.3739/rikusui.56.269

Flood, B., Wells, M., Dunlop, E., & Young, J. (2020). Internal waves pump waters in and out of a deep coastal embayment of a large lake. *Limnology & Oceanography*, *65*(2), 205–223. https://doi.org/10.1002/lno.11292

Foroughan, M., Hamze-Ziabari, S. M., Lemmin, U., & Barry, D. A. (2022). A persistent submesoscale frontal slick: A novel marker of the mesoscale flow field in a large lake (Lake Geneva). *Geophysical Research Letters*, *49*(20), e2022GL100262. https://doi.org/10.1029/2022GL100262

Gaillard, R., Perroud, M., Goyette, S., & Kasparian, J. (2022). Multi-column modelling of Lake Geneva for climate applications. *Scientific Reports*, *12*(1), 353. https://doi.org/10.1038/s41598-021-04061-6

Gill, A. (1982). Atmosphere-ocean dynamics. *International Geophysics*, *30*, 612. Elsevier.

Gula, J., Molemaker, M. J., & McWilliams, J. C. (2014). Submesoscale cold filaments in the Gulf Stream. *Journal of Physical Oceanography*, *44*(10), 2617–2643. https://doi.org/10.1175/JPO-D-14-0029.1

Gutiérrez, D., Bouloubassi, I., Sifeddine, A., Purca, S., Goubanova, K., Graco, M., et al. (2011). Coastal cooling and increased productivity in the main upwelling zone off Peru since the mid-twentieth century. *Geophysical Research Letters*, *38*(7), L07603. https://doi.org/10.1029/2010GL046324

Hamze-Ziabari, S. M., Foroughan, M., Lemmin, U., & Barry, D. A. (2022). Monitoring mesoscale to submesoscale processes in large lakes with Sentinel-1 SAR imagery: The Case of Lake Geneva. *Remote Sensing*, *14*(19), 4967. https://doi.org/10.3390/rs14194967

Hamze-Ziabari, S. M., Lemmin, U., Foroughan, M., Reiss, R. S., & Barry, D. A. (2023). Data for: Chimney-like intense pelagic upwelling in the center of basin-scale cyclonic gyres in large Lake Geneva [Dataset]. Zenodo. https://doi.org/10.5281/zenodo.7941268

Hamze-Ziabari, S. M., Lemmin, U., Soulignac, F., Foroughan, M., & Barry, D. A. (2022). Basin-Scale gyres and mesoscale eddies in large lakes: A novel procedure for their detection and characterization, assessed in Lake Geneva. *Geoscientific Model Development*, *15*(23), 8785–8807. https://doi.org/10.5194/gmd-15-8785-2022

Hamze-Ziabari, S. M., Razmi, A. M., Lemmin, U., & Barry, D. A. (2022c). Detecting submesoscale cold filaments in a basin-scale gyre in large, deep Lake Geneva (Switzerland/France). *Geophysical Research Letters*, *49*(4), e2021GL096185. https://doi.org/10.1029/2021GL096185

Hui, Y., Farnham, D. J., Atkinson, J. F., Zhu, Z., & Feng, Y. (2021). Circulation in Lake Ontario: Numerical and physical model analysis. *Journal of Hydraulic Engineering*, *147*(8), 05021004. https://doi.org/10.1061/(ASCE)HY.1943-7900.0001908

Hüsler, F., Fontana, F., Neuhaus, C., Riffler, M., Musial, J., & Wunderle, S. (2011). AVHRR archive and processing facility at the University of Bern: A comprehensive 1-km satellite data set for climate change studies. *EARSeL eProceedings*, *10*(2), 83–101.

Huttula, T., & Sarvala, J. (2012). Tanganyika Lake: Strong in hydrodynamics, diverse in ecology. In L. Bengtsson, R. W. Herschy, & R. W. Fairbridge (Eds.), *Encyclopedia of lakes and reservoirs. Encyclopedia of earth sciences series*. Springer. https://doi.org/10.1007/978-1-4020-4410-6_168

Ishikawa, K., Kumagai, M., Vincent, W. F., Tsujimura, S., & Nakahara, H. (2002). Transport and accumulation of bloom-forming cyanobacteria in a large, mid-latitude lake: The gyre-microcystis hypothesis. *Limnology*, *3*(2), 87–96. https://doi.org/10.1007/s102010200010

Jane, S. F., Hansen, G. J. A., Kraemer, B. M., Leavitt, P. R., Mincer, J. L., North, R. L., et al. (2021). Widespread deoxygenation of temperate lakes. *Nature*, *594*(7861), 66–70. https://doi.org/10.1038/s41586-021-03550-y

Ji, Z.-G., & Jin, K.-R. (2006). Gyres and seiches in a large and shallow lake. *Journal of Great Lakes Research*, *32*(4), 764–775. https://doi.org/10.3394/0380-1330(2006)32[764:GASIAL]2.0.CO;2

Kovalevsky, D. V., Bashmachnikov, I. L., & Alekseev, G. V. (2020). Formation and decay of a deep convective chimney. *Ocean Modelling*, *148*, 101583. https://doi.org/10.1016/j.ocemod.2020.101583

Large, G., & Yeager, S. (2004). Diurnal to decadal global forcing for ocean and sea-ice models: The data sets and flux climatologies. https://doi.org/10.5065/D6KK98Q6

Laval, B. E., Imberger, J., & Findikakis, A. N. (2005). Dynamics of a large tropical lake: Lake Maracaibo. *Aquatic Sciences*, *67*(3), 337–349. https://doi.org/10.1007/s00027-005-0778-1

Lemmin, U. (2016). Mouvements des masses d'eau (Water mass movement). In U. Lemmin (Ed.), *Dans les abysses du Léman (descent into the abyss of Lake Geneva)*. Presses Polytechniques et Universitaires Romandes.

Lemmin, U. (2020). Insights into the dynamics of the deep hypolimnion of Lake Geneva as revealed by long-term temperature, oxygen, and current measurements. *Limnology & Oceanography*, *65*(9), 2092–2107. https://doi.org/10.1002/lno.11441

Lemmin, U., & D'Adamo, N. (1996). Summertime winds and direct cyclonic circulation: Observations from Lake Geneva. *Annales Geophysicae*, *14*(11), 1207–1220. https://doi.org/10.1007/s00585-996-1207-z

Lemmin, U., Mortimer, C. H., & Bäuerle, E. (2005). Internal seiche dynamics in Lake Geneva. *Limnology & Oceanography*, *50*(1), 207–216. https://doi.org/10.4319/lo.2005.50.1.0207

Lovecchio, E., Gruber, N., Münnich, M., & Frenger, I. (2022). On the processes sustaining biological production in the offshore propagating eddies of the Northern Canary upwelling system. *Journal of Geophysical Research: Oceans*, *127*(2), e2021JC017691. https://doi.org/10.1029/2021JC017691

Lu, Z., Wang, G., & Shang, X. (2020). Strength and spatial structure of the perturbation induced by a tropical cyclone to the underlying eddies. *Journal of Geophysical Research: Oceans*, *125*(5), e2020JC016097. https://doi.org/10.1029/2020JC016097

Lv, M., Wang, F., Li, Y., Zhang, Z., & Zhu, Y. (2022). Structure of sea surface temperature anomaly induced by mesoscale eddies in the North Pacific Ocean. *Journal of Geophysical Research: Oceans*, *127*(3), e2021JC017581. https://doi.org/10.1029/2021JC017581

Marshall, J., Adcroft, A., Hill, C., Perelman, L., & Heisey, C. (1997). A finite-volume, incompressible Navier Stokes model for studies of the ocean on parallel computers. *Journal of Geophysical Research*, *102*(C3), 5753–5766. https://doi.org/10.1029/96JC02775

McKinney, P., Holt, B., & Matsumoto, K. (2012). Small eddies observed in Lake Superior using SAR and sea surface temperature imagery. *Journal of Great Lakes Research*, *38*(4), 786–797. https://doi.org/10.1016/j.jglr.2012.09.023

McWilliams, J. C. (2019). A survey of submesoscale currents. *Geoscience Letters*, *6*(1), 3. https://doi.org/10.1186/s40562-019-0133-3

Mortimer, C. H. (2004). *Lake Michigan in motion: Responses of an inland sea to weather, earth-spin, and human activities*. Univ of Wisconsin Press.

Ostrovsky, I., & Sukenik, A. (2008). Spatial heterogeneity of biogeochemical parameters in a subtropical lake. In P. K. Mohanty (Ed.), *Monitoring and modelling lakes and coastal environments* (pp. 79–90). Springer Netherlands. https://doi.org/10.1007/978-1-4020-6646-7_6

Pickett, M. H., & Paduan, J. D. (2003). Ekman transport and pumping in the California Current based on the U.S. Navy's high-resolution atmospheric model (COAMPS). *Journal of Geophysical Research*, *108*(C10), 3327. https://doi.org/10.1029/2003JC001902

Pisoni, J. P., Rivas, A. L., & Piola, A. R. (2014). Satellite remote sensing reveals coastal upwelling events in the San Matías Gulf—Northern Patagonia. *Remote Sensing of Environment*, *152*, 270–278. https://doi.org/10.1016/j.rse.2014.06.019

Plattner, S., Mason, D. M., Leshkevich, G. A., Schwab, D. J., & Rutherford, E. S. (2006). Classifying and forecasting coastal upwellings in Lake Michigan using satellite derived temperature images and buoy data. *Journal of Great Lakes Research*, *32*(1), 63–76. https://doi.org/10.3394/0380-1330(2006)32[63:CAFCUI]2.0.CO;2

Pöschke, F., Lewandowski, J., Engelhardt, C., Preuß, K., Oczipka, M., Ruhtz, T., & Kirillin, G. (2015). Upwelling of deep water during thermal stratification onset—A major mechanism of vertical transport in small temperate lakes in spring? *Water Resources Research*, *51*(12), 9612–9627. https://doi.org/10.1002/2015WR017579

Rahaghi, A. I., Lemmin, U., Cimatoribus, A., Bouffard, D., Riffler, M., Wunderle, S., & Barry, D. A. (2018). Improving surface heat flux estimation for a large lake through model optimization and two-point calibration: The case of Lake Geneva. *Limnology and Oceanography: Methods*, *16*(9), 576–593. https://doi.org/10.1002/lom3.10267

Rahaghi, A. I., Lemmin, U., Cimatoribus, A. A., & Barry, D. A. (2019). The importance of systematic spatial variability in the surface heat flux of a large lake: A multiannual analysis for Lake Geneva. *Water Resources Research*, *55*(12), 10248–10267. https://doi.org/10.1029/2019WR024954

Ralph, E. A. (2002). Scales and structures of large lake eddies. *Geophysical Research Letters*, *29*(24), 30–31. https://doi.org/10.1029/2001GL014654

Reiss, R. S., Lemmin, U., & Barry, D. A. (2022). Wind-induced hypolimnetic upwelling between the multi-depth basins of Lake Geneva during winter: An overlooked deepwater renewal mechanism? *Journal of Geophysical Research: Oceans*, *127*(6), e2021JC018023. https://doi.org/10.1029/2021JC018023

Reiss, R. S., Lemmin, U., & Barry, D. A. (2023). What role does stratification play during winter in wind-induced exchange between the multi-depth basins of a large lake (Lake Geneva)? *Journal of Great Lakes Research*, *49*(2), 406–421. https://doi.org/10.1016/j.jglr.2023.02.005

Reiss, R. S., Lemmin, U., Cimatoribus, A. A., & Barry, D. A. (2020). Wintertime coastal upwelling in Lake Geneva: An efficient transport process for deepwater renewal in a large, deep lake. *Journal of Geophysical Research: Oceans*, *125*(8), e2020JC016095. https://doi.org/10.1029/2020JC016095

Riffler, M., Lieberherr, G., & Wunderle, S. (2015). Lake surface water temperatures of European Alpine lakes (1989–2013) based on the Advanced Very High Resolution Radiometer (AVHRR) 1 km data set. *Earth System Science Data*, *7*(1), 1–17. https://doi.org/10.5194/essd-7-1-2015

Romanovsky, V. V., & Shabunin, G. D. (2002). Currents and vertical water exchange in Lake Issyk Kul. In J. Klerkx & B. Imanackunov (Eds.), *Lake Issyk-Kul: Its natural environment* (pp. 77–87). Springer Netherlands. https://doi.org/10.1007/978-94-010-0491-6_7

Rowe, M. D., Anderson, E. J., Beletsky, D., Stow, C. A., Moegling, S. D., Chaffin, J. D., et al. (2019). Coastal upwelling influences hypoxia spatial patterns and nearshore dynamics in Lake Erie. *Journal of Geophysical Research: Oceans*, *124*(8), 6154–6175. https://doi.org/10.1029/2019JC015192

Schwab, D. J., O'Connor, W. P., & Mellor, G. L. (1995). On the net cyclonic circulation in large stratified lakes. *Journal of Physical Oceanography*, *25*(6), 1516–1520. https://doi.org/10.1175/1520-0485(1995)025<1516:OTNCCI>2.0.CO;2

Schwab, D. J., & Beletsky, D. (2003). Relative effects of wind stress curl, topography, and stratification on large-scale circulation in Lake Michigan. *Journal of Geophysical Research*, *108*(C2), 3044. https://doi.org/10.1029/2001JC001066

Shimizu, K., Imberger, J., & Kumagai, M. (2007). Horizontal structure and excitation of primary motions in a strongly stratified lake. *Limnology & Oceanography*, *52*(6), 2641–2655. https://doi.org/10.4319/lo.2007.52.6.2641

Simons, T. J. (1980). *Circulation models of lakes and inland seas* (Vol. 203). Canadian Bulletin of Fisheries and Aquatic Sciences (Dept. of Fisheries and Oceans.146

Strub, P. T., & Powell, T. M. (1986). Wind-driven surface transport in stratified closed basins: Direct versus residual circulations. *Journal of Geophysical Research*, *91*(C7), 8497–8508. https://doi.org/10.1029/JC091iC07p08497

Troitskaya, E., Blinov, V., Ivanov, V., Zhdanov, A., Gnatovsky, R., Sutyrina, E., & Shimaraev, M. (2015). Cyclonic circulation and upwelling in Lake Baikal. *Aquatic Sciences*, *77*(2), 171–182. https://doi.org/10.1007/s00027-014-0361-8

Valbuena, S. A., Bombardelli, F. A., Cortés, A., Largier, J. L., Roberts, D. C., Forrest, A. L., & Schladow, S. G. (2022). 3D flow structures during upwelling events in lakes of moderate size. *Water Resources Research*, *58*(3), e2021WR030666. https://doi.org/10.1029/2021WR030666

Valerio, G., Cantelli, A., Monti, P., & Leuzzi, G. (2017). A modeling approach to identify the effective forcing exerted by wind on a prealpine lake surrounded by a complex topography. *Water Resources Research*, *53*(5), 4036–4052. https://doi.org/10.1002/2016WR020335

Vallis, G. K. (2017). *Atmospheric and oceanic fluid dynamics: Fundamentals and large-scale circulation* (2nd ed.). Cambridge University Press. https://doi.org/10.1017/9781107588417

Voudouri, A., Avgoustoglou, E., & Kaufmann, P. (2017). Impacts of observational data assimilation on operational forecasts. In T. Karacostas, A. Bais, & P. T. Nastos (Eds.), *Perspectives on atmospheric sciences* (pp. 143–149). Springer International Publishing. https://doi.org/10.1007/978-3-319-35095-0_21

Wang, B., & An, S.-I. (2005). A method for detecting season-dependent modes of climate variability: S-EOF analysis. *Geophysical Research Letters*, *32*(15), L15710. https://doi.org/10.1029/2005GL022709

Xu, W., Collingsworth, P. D., & Minsker, B. (2019). Algorithmic characterization of lake stratification and deep chlorophyll layers from depth profiling water quality data. *Water Resources Research*, *55*(5), 3815–3834. https://doi.org/10.1029/2018WR023975

Zhang, Z., Qiu, B., Klein, P., & Travis, S. (2019). The influence of geostrophic strain on oceanic ageostrophic motion and surface chlorophyll. *Nature Communications*, *10*(1), 2838. https://doi.org/10.1038/s41467-019-10883-w